ELSEVIER

Precambrian Research 84 (1997) 37–62

Precambrian Research

Chemical diversity and origin of Precambrian charnockitic rocks of the central Pedlar massif, Grenvillian Blue Ridge Terrane, Virginia

S.S. Hughes [a,*], S.E. Lewis [b], M.J. Bartholomew [c], A.K. Sinha [d], T.A. Hudson [e], N. Herz [f]

[a] *Department of Geology, Idaho State University, Pocatello, ID 83209, USA*
[b] *Earth Sciences and Resources Institute, University of South Carolina, Columbia, SC 29208, USA*
[c] *Earth Sciences and Resources Institute, University of South Carolina, Columbia, SC 29208, USA*
[d] *Department of Geological Sciences, Virginia Tech, Blacksburg, VA 24061, USA*
[e] *Chevron USA Corp., New Orleans, LA 70122, USA*
[f] *Department of Geology, University of Georgia, Athens, GA 30602, Greece*

Received 25 March 1996; accepted 12 February 1997

Abstract

Middle Proterozoic rocks of the Pedlar massif are comprised of varied charnockitic and granulitic lithologies representing ~1150–1000 Ma Grenvillian metamorphic and igneous events in the central Appalachians of Virginia. Chemically and mineralogically diverse units include metaluminous to peraluminous charnockites, enderbites, jotunites and granulite gneisses ranging in SiO_2 from 47 to 79 wt.%. Relative to bulk continental crust, typical charnockites are enriched by ~3-6× in Rb, K, Ba, LREE, Zr and Hf, less enriched in Ta, Sr, P and HREE, and depleted in Cs, Th, Ti and Sc, although low-SiO_2 members have relatively high Ti and P and some high-SiO_2 units are depleted in K, Rb and Ba. The Pedlar River Charnockite Suite (PRCS), Vesuvius megacrystic charnockite (VMC), Nellysford Granulite Gneiss (NGG) and the Lady Slipper Granulite Gneiss (LSGG) exhibit common chemical signatures and trends, notably evident in uniform LREE-enriched patterns with variable Eu anomalies, which reflect their derivation from a mixed protolith of volcanics and reworked volcaniclastic sediments dated at ~1130–1150 Ma. Pedlar River charnockites represent portions of deep-seated granulite gneisses that were mobilized by granulite facies dehydration melting and emplaced en masse as plutons into overlying and surrounding gneisses during the Grenville episode. Divergent REE patterns in the PRCS are attributed to crystallization of quartz, feldspar ± garnet, or HREE-compatible mafic and accessory phases leading to complementary chemical signatures in mafic and felsic layers.

Depletion of Cs throughout the Pedlar massif is attributed to its incompatibility with major mineral phases during either protolith evolution or granulite facies dehydration, while dispersions in K, Rb, Sr, Ba and Eu are due to the relative proportions of the major phases quartz, K-feldspar, plagioclase and biotite. Mobility of insoluble trace elements Zr, Hf, Ta and Th require partial melting and crystallization of accessory mineral phases, whereas Sc, Cr and REE mobility depends on the proportions of pyroxene and garnet. Several leucocharnockites and other felsic rocks of the PRCS show markedly elevated Th values ranging from ~10 to 83 ppm which complement depleted Th in typical PRCS units. These charnockitic rocks represent low-degree partial melts (~1–5%) from normal PRCS or NGG protoliths to produce high-silica magmas which separated from the main charnockitic body. © 1997 Elsevier Science B.V.

Keywords: Charnockite; Granulite facies; Proterozoic; Grenville orogeny

* Corresponding author. Tel: 208-236-4387; Fax: 208-236-4414; e-mail: hughscot@ux1.isu.edu

0301-9268/97/$17.00 © 1997 Elsevier Science B.V. All rights reserved.
PII S0301-9268(97)00015-6

1. Introduction

In the Blue Ridge Province of the central and northern Virginia Appalachians, middle Proterozoic rocks comprise a variety of terranes and tectonic subdivisions that were involved in the Grenville orogeny. Initial interpretations of geochemical signatures and layering textures suggest a calc-alkaline magmatic arc protolith consisting of differentiated volcanic or volcaniclastic sequences (Sinha and Bartholomew, 1984; Bartholomew et al., 1991). Radiometric age relations suggest that the magmatic system was active up to the culminating Grenville event, and coupled with field and geochemical data permit the separation of the Virginia Blue Ridge Grenville into two massifs: Pedlar and Lovingston. These are separated by a major Paleozoic fault (Rockfish Valley fault). In this report we present data for rocks associated with the Pedlar massif.

Published geochemical evaluation of both massifs include primarily major element and few trace element abundances (Ames, 1981; Hudson, 1981; Sinha and Bartholomew, 1984; Herz, 1984; Herz and Force, 1984). Nonetheless, major oxide distributions in the Blue Ridge basement rocks can be grossly but reasonably interpreted to represent a Proterozoic volcanic/plutonic complex. However, trace element data, in addition to existing major element data is necessary to evaluate possible compositional effects of granulite facies metamorphism and to develop a more rigorous geochemical signature useful to delineate massifs which have experienced different Grenville and Paleozoic histories, e.g. Pedlar and Lovingston massifs. This research is part of an effort to compile existing major element data with new trace element abundances determined by instrumental neutron activation analysis (INAA) in order to provide more complete datasets for the Pedlar and Lovingston massifs. In this paper, we examine major and trace element signatures within charnockites, granulite gneisses and related rocks of the Pedlar massif which forms the western part of the Grenvillian Blue Ridge Terrane. Chemical and lithologic variations are evaluated for probable protoliths and petrologic processes involved in granulite facies metamorphism and associated plutonism. Implications for lower crustal evolution are emphasized by comparisons with predicted average crustal compositions and timing of the Grenville orogeny.

2. The Pedlar massif: geological setting and rock associations

Deep crust is represented by two major massifs (Fig. 1) of the Middle Proterozoic Blue Ridge Terrane (Bartholomew and Lewis, 1992) exposed in the core of the Blue Ridge anticlinorium, a major Paleozoic fold related to late Paleozoic (Alleghanian) thrusting in the central Virgina Appalachians (Mitra and Elliott, 1980; Mitra and Lukert, 1982; Evans, 1989). The Pedlar and Lovingston massifs, initially characterized by Bartholomew (1977); Bartholomew (1981) and Bartholomew et al. (1981), lie north-west and south-east of the Rockfish Valley fault zone (Fig. 1), a Paleozoic fault which dies out northeastward within the core of the Blue Ridge anticlinorium (Bartholomew and Lewis, 1984; Bailey and Simpson, 1993). The massifs include igneous and granulite facies metamorphic rocks, formed during Grenville orogensis, which were then subjected to late Proterozoic and Paleozoic lower-greenschist metamorphism (e.g. Sinha and Bartholomew, 1984; Evans, 1991). These Blue Ridge massifs are distinguished one from the other by their contrasting rock associations, different petrologic and structural evolutions, and by physiographic aspects that reflect those lithologic assemblages (e.g. Bartholomew et al., 1991).

A major angular unconformity separates Grenville basement rocks from overlying Late Proterozoic Catoctin Formation volcanics that erupted during Late Proterozoic Iapetus rifting between North America and Baltica. U–Pb ages of ~700–730 Ma were initially reported for this event (e.g. Sinha and Bartholomew, 1984), but the Catoctin lavas were subsequently dated at ~570 Ma (Badger and Sinha, 1988; Aleinikoff et al., 1995). Tollo and Hutson (1996) suggest a wide-scale extensional regime along the Laurentian margin throughout which ongoing magmatism ensued about 130 Ma before the breakup. Bailey

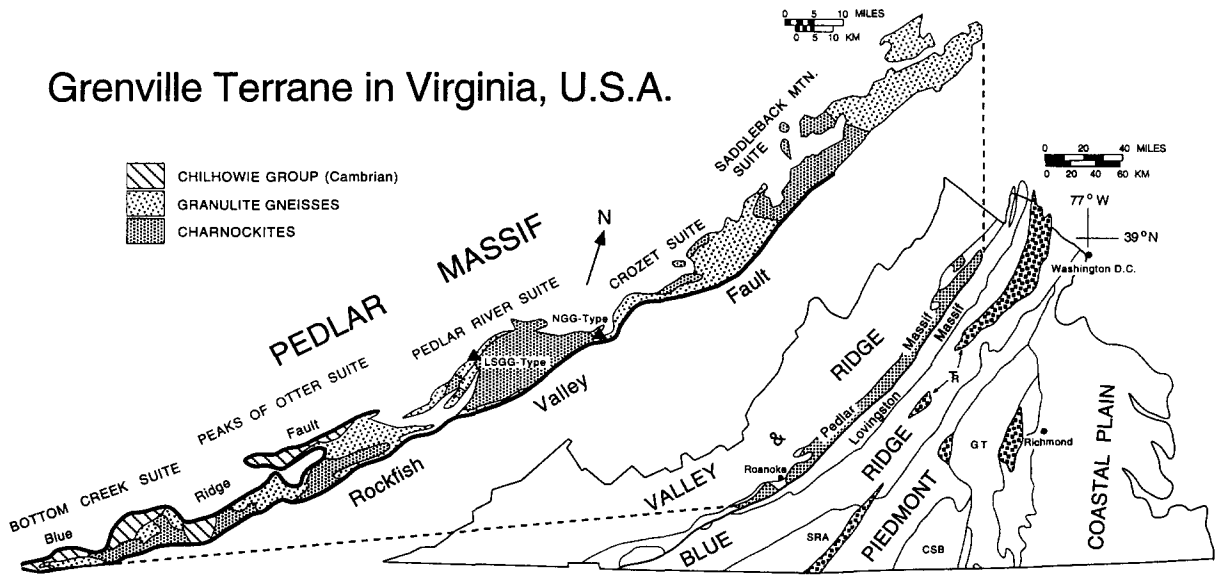


Fig. 1. Simplified geologic map of Proterozoic massifs in the Grenvillian Blue Ridge of Virginia, eastern U.S.A. The Rockfish Valley fault separates two major terranes, the Pedlar and Lovingston massifs, comprised of granulite facies rocks, both of which were subjected to Paleozoic lower-greenschist metamorphism and exhumed during Late Paleozoic thrusting. The Pedlar River Suite is one of five charnockitic plutonic suites in the Pedlar massif intruded into granulite gneisses. Filled triangles indicate type localities of the Lady Slipper (LSGG) and Nellysford (NGG) granulite gneisses. The Piedmont geologic province consists of terranes accreted during Paleozoic orogenesis, e.g. Goochland Terrane (GT), Smith River allochthon (SRA), and Carolina Slate Belt (CSB). Mesozoic rift basins (T_R) are associated with the opening of the Atlantic Ocean.

and Simpson (1993) documented the structural differences, under greenschist facies conditions, between Iapetan extension, which is prevalent in the Lovingston massif, and subsequent Paleozoic thrusting. Paleozoic metamorphism occurred at 425–450 Ma according to K–Ar, U–Pb and Rb–Sr data summarized by Bartholomew et al. (1991). This Ordovician–Silurian event likely produced chlorite/actinolite/biotite foliation in the Catoctin cover sequence as well as chlorite/biotite foliation in the Blue Ridge Basement (Bartholomew et al., 1981; Evans, 1991). Subsequent retrograde, subgreenschist-facies metamorphism at 303–273 Ma (Elliot and Aronson, 1987) was concomitant with Late Paleozoic thrusting and likely contributed to disturbance of Ordovician K–Ar systematics in the late Paleozoic. Although the deep crustal rocks of the Blue Ridge were subjected to several periods of low-grade regional metamorphism and deformation, the charnockites and granulite-facies gneisses within the Pedlar massif typically exhibit fewer effects of these retrograde events than the rocks of the Lovingston massif.

The Pedlar River Charnockite Suite (Fig. 1) is one of five charnockitic plutonic suites intruded into granulite gneisses of the Pedlar massif (Bartholomew and Lewis, 1984). The rock units (excluding names) as mapped by Bartholomew and Lewis (1984) were used with minor modification by the Virginia Division of Mineral Resources (1993) for the Blue Ridge portion of the most recent geologic map of Virginia. In the central Pedlar massif (Fig. 2), these rock units include: primarily charnockites of the Pedlar River Charnockite Suite (PRCS); the Vesuvius megacrystic charnockite (VMC) which is a megacrystic K-feldspar charnockite of the PRCS; the Nellysford Granulite Gneiss (NGG); quartzofeldspathic and biotite–hypersthene gneisses, the latter of which represents the Lady Slipper Granulite Gneiss (LSGG); and a small body of noritic granulite (sample 344A) that represents an appa-

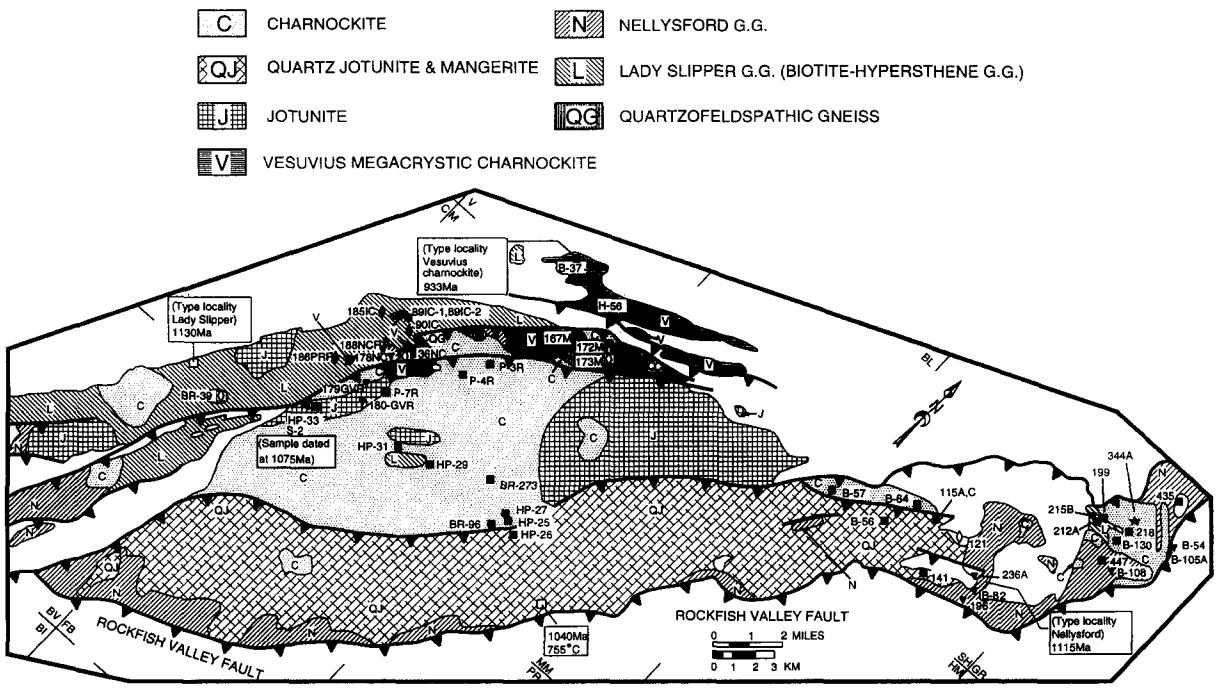


Fig. 2. Geologic map of the Pedlar River Suite segment of the Pedlar massif in the central Blue Ridge, Virginia, showing locations of geochemical samples used in this study (compiled from Bartholomew, 1977; Hudson, 1981; Herz and Force, 1984; and Sinha and Bartholomew, 1984). Symbols are the same as those given in Fig. 3. Boundaries are shown for 1:24 000-scale U.S. Geological Survey 7.5-minute quadrangle maps used for geologic mapping and sample locations provided in Table 4: Big Island (BI), Big Levels (BL), Buena Vista (BV), Cornwall (C), Forks of Buffalo (FB), Greenfield (GR), Horseshoe Mountain (HM), Massies Mill (MM), Montebello (M), Piney River (PR), Sherando (SH), and Vesuvius (V). See Fig. 1 for geologic relation of this segment to the remainder of the Pedlar massif.

rently rather isolated and enigmatic mafic unit in the Pedlar massif.

The timing of Grenville events in the Pedlar massif is based specifically on U–Pb, Rb–Sr, and Nd–Sm systematics of rocks in the area of study (Figs. 1 and 2). Bartholomew et al. (1991), on the basis of field relations, interpreted the data to represent diachronous intrusion of charnockites and other plutons at ~1050 Ma into ~1130 Ma country rocks followed by the culmination of Grenvillian metamorphism in the Blue Ridge Terrane at ~1000 Ma. Sinha and Bartholomew (1984) reported a U–Pb concordia protolith of age 1130 Ma for euhedral zircons of the Lady Slipper Granulite and A.K. Sinha (unpublished data) obtained a preliminary protolith age of ~1115 Ma for the Nellysford Granulite Gneiss. Sinha and Bartholomew (1984) reported a U–Pb age of 1075 Ma for emplacement of the Pedlar River Charnockite Suite. Herz and Force (1984) reported a zircon Pb–Pb age of 1040 Ma for a charnockite of the PRCS as well. A Sm–Nd whole-rock isochron age of 1489 ± 118 Ma for the PRCS (Pettingill et al., 1984) suggests the presence of inherited older crust in the charnockite source region. The Pettingill et al. (1984) whole rock Rb–Sr isochron age of 1021 ± 36 Ma for the Pedlar River Charnockite Suite may represent a partial re-equilibration of Rb–Sr in this suite to Grenville metamorphism. The time of Grenville metamorphism, however, is firmly established by the coincidence of a 1009 ± 26 Ma Rb–Sr isochron age with the Sm–Nd isochron age of 1004 ± 36 Ma for ferrodiorites/quartz monzonite plutons of the Lovingston massif (Pettingill et al., 1984), which have a 1100 Ma zircon U–Pb age of emplacement

(Sinha and Bartholomew, 1984). These data support a protracted, complex history of granulite facies metamorphism occurring over periods of up to several hundred Ma (Bohlen and Mezger, 1989; Mezger et al., 1993).

Herz (1984) obtained a temperature of ~760°C for one orthopyroxene–clinopyroxene pair in a Pedlar charnockite (Fig. 2). This implies equilibration above the dry solidus (~720–750°C @ 20–25 km) of muscovite granite (Huang and Wyllie, 1973) equivalent to ultrametamorphism (White and Chappell, 1977) although it is too low to support extensive partial melting. It is consistent with the ubiquitous occurrence of hypersthene + almandine (with $Py_{16-19}Gr_{8-16}Sp_2$; Evans, 1991) assemblages in different units throughout the eastern part of the Pedlar massif in this region (Fig. 2). The assemblage is characteristic of the deeper crustal granulite facies (Bohlen and Mezger, 1989). However, in the north-western part of the massif, garnet is generally absent and hypersthene coexists with hornblende. This suggests either local subsolidus conditions (Patiño-Douce and Beard, 1995) and/or possible local variation in source composition relative to the eastern part of the massif (Bartholomew et al., 1981).

2.1. Pedlar River Charnockite Suite

The Pedlar River Charnockite Suite was identified by Bartholomew et al. (1981) based on 1:24 000-scale mapping (Bartholomew, 1977), but formally named later. Following Streckeisen (1974), Streckeisen (1976) nomenclature the suite includes the major charnockite lithologies (farsundite and jotunite) as well as mafic-poor variants (leucocharnockite) and the Vesuvius megacrystic charnockite (Bartholomew and Lewis, 1984; Sinha and Bartholomew, 1984). These plutonic bodies are typically greenish gray, coarse-grained, massive to poorly-foliated rocks composed primarily of large green to white perthitic feldspar with variable amounts of plagioclase, quartz, orthopyroxene, clinopyroxene, garnet, and minor hornblende. Accessory minerals include sphene, zircon and apatite. Plagioclase of andesine composition and relict igneous hypidiomorphic granular textures are typical. Field relations show that the PRCS rocks intruded the granulite gneiss country rock (Bartholomew and Lewis, 1984). Within the main portion of the suite, the lithology changes from medium-grained charnockite near the margin to increasingly coarser-grained charnockite, and ultimately leucocharnockite in the interior. The Vesuvius charnockite contains large (10 cm) crudely aligned K-feldspar phenocrysts, plagioclase (An_{42-46}), quartz, hornblende, and ilmenite with minor hypersthene, clinopyroxene, biotite and apatite.

Compositional layering occurs locally within the PRCS (Bartholomew, 1977), and is defined by thin (2–18 cm) to thick (>1 m), alternating mafic (higher ratio of pyroxene to plagioclase) and felsic layers that are finer-grained than the surrounding PRCS charnockite. These zones comprise pods and lenses up to several tens of meters in length, and occur well within the charnockite bodies away from gneissic country rock. It is not clear from field studies whether they represent far-removed gneissic xenoliths, primary layering in the protolith, or compositional segregations produced during granulite facies metamorphism. Such centimeter-scale layering is common in the north-eastern part of the PRCS (Fig. 2) in poorly-exposed, fine-grained, lensoidal mafic bodies that are similar to mafic cumulates. Numerous sill-like bodies of massive ilmenite–hornblende gneiss also occur within the Vesuvius charnockite and as discordant dike-like bodies in the adjacent layered granulite gneiss (Hudson, 1981).

Mafic granulites are occasionally associated with the charnockite suites of the Pedlar massif as small dike-like bodies (Bartholomew, 1977, Bartholomew, 1981; Bartholomew et al., 1991). Only one noritic granulite has been mapped within the area (sample 344A); it has a xenomorphic-granular texture throughout and the margin is finer grained than the interior. The rock is primarily clinopyroxene and orthopyroxene with minor spinel, magnetite and zoned andesine.

2.2. Granulite gneisses

The LSGG, named and described by Sinha and Bartholomew (1984), is a light greenish gray, fine- to medium-grained, foliated to massive granoblas-

tic gneiss, containing plagioclase (An_{40}), quartz, hypersthene, garnet and biotite. Discontinuous 1–3 mm aggregates of pyroxene and biotite give this gneiss a distinctive striped or streaky foliation; hence it is referred to here as biotite–hypersthene gneiss. The NGG, described by Bartholomew (1977, 1981), is a dark greenish gray, well-layered (cm-scale), fine- to medium-grained, charnockitic gneiss with a granoblastic texture. Plagioclase (An_{42}), perthitic feldspar, quartz, orthopyroxene and garnet are the major minerals present along with minor retrograde greenschist-facies minerals. Commonly associated with NGG and LSGG is a massive to poorly-foliated, fine- to medium-grained, quartzofeldspathic gneiss composed primarily of perthitic feldspar with quartz and plagioclase but containing a very minor amount of mafic minerals. The quartzofeldspathic gneiss essentially has a granoblastic texture and the foliation is primarily due to alignment of elongated feldspar and quartz grains.

3. Geochemistry

Aliquots of samples previously analyzed for major elements over the past two decades were used for INAA in order to maintain consistency among various petrologic studies, but a few of the analyses required resampling the outcrop. Elemental standards included N.I.S.T. Reference Material 1633a (coal fly ash); U.S. Geological Survey standards (or in-house equivalents) BCR-1, BHVO-1, GSP-1; and an aliquot of the Allende meteorite. Powdered (~0.8 g) samples of rocks and standards were irradiated for 6 h in the Oregon State University megawatt TRIGA Reactor and sequentially counted in high resolution Ge(Li) or HPGe gamma spectroscopy systems at the Oregon facility, others were counted in the INAA lab at Idaho State University.

Instrumental analytical precision (statistical error), combined with estimates of accuracy based on analysis of known materials, yielded total uncertainties of 1–2% for Na (as Na_2O), Fe (as FeO), Sc, Co, La and Sm; 2–4% for Ce, Eu, Yb, Hf and Th; 4–8% for Cr, Rb, Nd, Tb, Lu and Ta; 10–20% for Ba and Cs; and 20–40% for Ni, Sr, Zr and U. Significant figures for the reported values (Tables 1–3) reflect the analytical uncertainties during INAA or estimated uncertainties for major oxides. Although most samples were pulverized in a clean alumina-plate grinder, Co and Ta are not reported for samples for which powders had been prepared previously in a tungsten-carbide pulverizer. Rb and Sr data for two PRCS samples, BR-273 and HP-25, are from Pettingill et al. (1984) due to higher precision by X-ray fluorescence analysis for those elements.

Major element values were derived from published or unpublished data used in previous studies (Hudson, 1981; Sinha and Bartholomew, 1984). Internal consistency between INAA and reported major element abundances were maintained by matching data for Fe, Na, and other elements, if available.

Chemical analyses characterizing a significant portion of the Pedlar massif (Table 1) were obtained for 31 samples of the PRCS: 20 charnockites, and leucocharnockites, 8 layered charnockites, and 3 Versuvius megacrystic charnockites; and 17 samples of granulite gneiss: 10 NGG samples, 3 biotite–hypersthene (BH) gneiss (=LSGG), and 4 quartzofeldspathic (QF) gneiss samples. A single sample of noritic mafic granulite was analyzed. Sample locations referenced to U.S. Geological Survey 1:24 000- scale 7.5 minute quadrangle maps are provided in Table 4.

3.1. Major elements

Major oxide abundances cover a range in SiO_2 from ~49 to 77 wt.%, except the noritic granulite. Possible chemical dispersion related to Paleozoic deformation and retrograde alteration is not apparent. For example, three samples shown on the K_2O plot (435, HP-25 and B-64) were obtained from retrograded shear zones in the massif, whereas sample HP-27 is the undeformed equivalent of HP-25. These compositions show no significant dispersion from the overall trend and the chemical affinity of HP-25 to HP-27 is apparent.

A/CNK (molar $Al_2O_3/[CaO + Na_2O + K_2O]$) ratios range from metaluminous to peraluminous (Fig. 3) Most PRCS compositions yield A/CNK ratios less than 1.1 suggesting either I-type

Table 1
Chemical compositions of representative samples from the Pedlar massif

Type:	Pedlar River Charnockite Suite (PRCS)																
Sample:	B-56	180-GVR	BR-273	BR-96	HP-25	HP-26	HP-27	HP-29	HP-33	P-3R	P-4R	199	B-57	212A	B-64	HP-31	P-7R
[1]Ref:	3	1	2	2	2	2	2	2	2	1	1	3	3	3	3	2	1
Wt.%	Major Oxides Normalized to 100%																
SiO_2	69.2	54.0	67.7	55.1	66.1	55.9	64.7	65.7	67.0	69.7	67.9	72.8	73.0	73.1	76.1	68.9	66.2
TiO_2	0.99	1.80	0.54	2.82	0.63	2.60	0.94	0.85	0.88	0.49	0.60	0.15	0.37	0.36	0.13	0.66	0.60
Al_2O_3	13.0	17.9	16.2	14.8	15.7	14.3	15.1	16.4	15.0	15.1	14.5	14.3	13.4	13.4	12.7	14.5	15.6
FeO^*	6.01	8.70	3.43	9.64	4.81	10.8	6.23	4.20	4.98	2.52	4.56	2.44	2.77	4.01	2.36	4.45	5.76
MnO	0.08	0.05	0.06	0.13	0.07	0.13	0.09	0.06	0.05	0.03	0.03	0.01	0.04	0.02	0.02	0.06	0.04
MgO	0.74	1.48	0.46	3.81	0.66	4.51	0.88	1.22	1.26	0.46	0.43	0.46	0.37	0.43	0.20	1.43	0.55
CaO	2.39	7.22	3.02	6.52	3.31	5.54	3.59	2.49	2.76	2.17	3.26	0.10	1.31	0.74	0.22	2.07	2.51
Na_2O	2.02	5.07	3.22	3.08	2.83	2.88	2.53	3.32	2.98	3.82	3.78	3.31	2.92	2.93	3.22	2.96	3.04
K_2O	4.98	2.15	4.99	2.65	5.48	2.34	5.42	5.20	4.68	5.46	4.49	6.17	5.63	4.94	5.08	4.81	5.32
P_2O_5	0.58	1.55	0.39	1.43	0.39	1.14	0.53	0.54	0.38	0.30	0.37	0.16	0.22	0.10	0.02	0.13	0.45
Orig. Sum	100.5	100.3	101.0	99.6	99.3	101.3	98.5	99.2	99.5	100.1	99.8	99.7	99.5	100.4	100.4	99.4	98.3
ppm	Trace Elements by INAA																
Sc	12.2	21.6	7.3	22.7	11.1	23.7	14.7	10.2	14.9	3.7	9.3	4.7	1.2	5.8	2.7	10.8	3.5
Cr	4	10	4	58	3	75	3	7	10	4	5	3	3	8	4	27	3
Co	5.0	12.3	-	-	-	-	-	-	-	2.7	3.3	1.3	2.6	3.0	0.8	-	1.2
Ni	25	10	15	30	20	20	30	20	15	20	15	-	-	-	-	5	2
Rb	104	32	**134***	57	**125***	54	127	170	170	214	252	237	250	227	167	220	290
Cs	0.20	0.19	0.57	0.11	0.19	0.08	0.29	0.40	0.43	0.31	0.52	0.39	0.21	0.39	0.12	0.58	0.15
Sr	420	1050	**426***	440	**459***	360	480	480	310	590	550	140	270	150	170	100	185
Ba	1860	1390	1820	1330	2220	1300	2120	1570	1230	1570	2350	400	670	550	650	610	560
La	36.8	99.7	70.2	68.4	47.2	73.1	51.0	77.7	66.9	72.8	65.4	18.8	78.7	64.2	100	149	98.4
Ce	74.1	229	137	158	98.3	175	107	174	146	152	155	34.5	137	120	176	321	200
Nd	42	125	68	94	47	100	54	79	75	73	80	15	46	56	68	129	78
Sm	8.99	24.5	13.6	20.3	10.3	19.5	12.3	21.0	15.4	13.1	15.8	2.83	6.81	10.0	10.1	25.0	13.7
Eu	4.61	5.89	3.84	4.18	4.64	4.35	4.69	3.50	3.11	3.16	4.46	0.76	1.49	1.09	0.82	1.63	1.16
Tb	1.24	2.93	1.41	2.34	1.27	2.53	1.41	2.70	1.87	1.24	1.83	0.23	0.42	1.31	0.53	2.05	0.98
Yb	2.74	5.44	2.95	5.00	2.65	4.99	3.19	4.65	1.97	2.20	4.17	0.32	0.84	2.31	0.64	2.60	0.91
Lu	0.40	0.66	0.40	0.74	0.32	0.67	0.42	0.62	0.24	0.25	0.51	0.04	0.11	0.29	0.08	0.36	0.16
Zr	770	570	440	400	500	450	650	400	450	340	530	120	140	150	140	300	240
Hf	33.8	13.7	14.9	13.4	18.2	13.7	25.3	14.7	17.4	10.4	16.1	4.6	7.2	7.8	7.4	16.6	8.2
Ta	0.51	1.52	-	-	-	-	-	-	-	1.16	1.92	0.16	0.13	0.79	0.66	-	0.17
Th	0.4	2.5	1.0	1.3	2.2	2.1	1.2	1.6	5.4	0.4	0.6	15.0	25.2	19.1	54.6	83.4	54.4
U	-	0.5	1.7	1.2	0.7	1.1	0.8	1.5	1.9	1.0	1.0	10.7	3.3	1.6	4.4	4.2	4.5

Table 2

Type	Pedlar River Charnockite Suite (PRCS)											Vesuvius Megacr. Charn.			Nellysford Gran. Gneiss		
Sample	172M	B-130	S-2	115A	115C	435	218	141	447	891C-1	891C-2	167M	B-37	H-56	178NC	179-GVR	188-NCR
ref	1	3		3	3	3	3	3	3	1		1	3		1	1	
Wt.%																	
SiO_2	60.5	73.3	-	61.1	69.6	63.1	72.2	70.4	66.9	64.0	-	59.0	65.1	64.7	67.0	49.3	-
TiO_2	1.56	0.75	-	1.50	0.96	1.31	1.33	0.67	1.19	1.65	-	1.21	0.99	1.03	0.73	3.49	-
Al_2O_3	16.3	12.7	-	14.0	11.7	14.7	12.4	13.9	12.4	13.1	-	17.1	14.2	15.4	14.6	15.5	-
FeO*	8.01	4.83	5.35	10.2	8.00	7.59	5.26	4.10	9.57	8.18	6.22	7.69	7.06	5.74	5.79	12.2	9.70
MnO	0.05	0.07	-	0.13	0.10	0.12	0.09	0.04	0.18	0.05	-	0.04	0.06	0.04	0.04	0.06	-
MgO	1.41	1.75	-	1.04	2.45	1.71	2.26	0.86	2.49	1.24	-	0.92	0.86	0.86	1.07	3.75	-
CaO	5.52	1.40	-	4.48	2.27	3.43	2.16	1.71	3.09	3.86	-	5.65	3.67	4.52	3.14	8.55	-
Na_2O	3.56	2.59	3.22	2.79	2.55	2.53	1.38	2.86	2.46	2.36	1.18	4.50	2.73	2.99	2.99	3.11	2.81
K_2O	2.04	2.40	-	4.07	2.21	4.94	2.70	5.12	1.59	3.76	-	3.12	4.76	4.11	4.41	1.48	-
P_2O_5	1.02	0.15	-	0.76	0.17	0.49	0.26	0.33	0.11	1.77	-	0.76	0.60	0.59	0.25	2.57	-
Orig. Sum	99.2	99.8	102.5	101.0	99.1	98.5	97.8	100.5	99.8	99.7	100.9	100.3	99.6	95.7			
ppm																	
Sc	17.7	11.4	14.1	21.6	20.4	25.1	12.9	13.4	25.8	21.3	17.6	18.1	25.1	7.8	17.1	23.8	29.8
Cr	11	63	11	7	107	43	100	15	135	6	8	-	12	5	39	59	65
Co	12.3	7.9	-	12.0	16.6	16.7	18.5	4.9	31.2	8.8	2.1	9.8	9.2	4.7	12.2	26.6	21.8
Ni	50	45	-	30	35	-	75	20	65	30	20	60	25	40	20	30	30
Rb	90	96	121	81	52	102	78	141	68	64	117	45	129	170	137	32	112
Cs	0.33	-	0.38	-	0.25	0.18	0.11	0.30	0.17	0.21	0.05	0.35	0.61	0.95	0.50	0.58	0.38
Sr	610	250	390	520	130	200	-	290	100	400	1050	670	700	680	220	890	130
Ba	1060	470	870	1550	640	1070	440	940	610	1670	1620	1310	2040	2850	890	850	630
La	92.1	528	82.0	74.9	41.6	53.0	92.8	34.7	59.5	99.4	98.5	56.2	89.8	53.9	78.4	80.5	94.3
Ce	201	-	175	171	80.0	105	159	62.4	90.4	237	186	132	207	113	151	191	212
Nd	103	460	87	98	30	66	72	29	51	129	109	63	102	60	67	108	96
Sm	20.5	76.2	17.6	23.7	5.54	13.8	14.2	6.80	10.9	26.5	25.7	14.1	21.7	12.3	13.1	21.5	19.8
Eu	5.04	9.52	2.87	5.28	1.68	2.12	2.44	1.79	3.91	4.80	5.14	5.31	4.78	4.63	2.03	4.90	1.70
Tb	2.94	9.34	2.04	3.02	0.91	1.94	2.41	1.05	4.37	3.10	2.72	1.91	2.50	1.67	1.59	2.41	2.72
Yb	4.71	32.1	2.18	6.73	4.95	5.23	9.34	4.36	30.7	6.70	6.37	4.20	5.06	2.71	3.85	4.30	6.70
Lu	0.69	4.48	0.30	0.94	0.78	0.82	1.47	0.66	4.55	0.85	0.84	0.54	0.67	0.32	0.54	0.57	0.92
Zr	320	230	550	420	180	270	300	200	230	950	1050	360	430	280	350	270	580
Hf	19.3	5.8	20.7	18.1	8.9	16.8	14.9	10.2	10.1	29.0	32.6	25.8	18.1	8.7	12.5	6.3	22.0
Ta	1.39	1.20	-	1.80	0.69	1.12	1.80	0.84	1.20	1.32	0.86	1.21	1.60	0.61	0.97	1.47	1.44
Th	37.2	19.1	16.9	0.8	4.1	0.7	1.9	0.3	10.9	0.2	-	1.2	2.9	1.6	12.6	1.8	7.9
U	10.0	4.8	2.3	-	-	1.6	2.1	-	1.4	0.1	0.7	1.1	1.5	0.8	0.9	1.0	1.2

Table 3

Type	Nellysford Granulite Gneiss							Biot.-Hypersthene Gneiss			Quartzofeldspathic Gneiss				Norite
Sample	196	215B	236A	B-105A	B-108	B-54	B-82	185-IC	186-PRR	90-IC	136-NC	121	173M	BR-39	344A
Ref	3	3	3	3	3	3	3	1	1	1	1	3	1	2	3
Wt.%															
SiO_2	72.1	63.3	70.1	63.9	56.1	52.4	64.1	68.7	73.4	70.7	76.4	76.1	77.2	76.2	44.8
TiO_2	0.37	1.22	0.68	0.98	1.97	1.97	1.10	0.75	0.52	0.53	0.02	0.13	0.29	0.06	0.43
Al_2O_3	14.2	15.3	12.5	14.0	15.7	18.0	14.5	14.4	13.6	13.9	12.7	12.9	12.2	12.1	14.8
FeO*	3.21	9.21	6.36	10.0	12.4	10.6	8.47	4.85	2.08	4.01	0.91	1.74	1.08	2.31	11.9
MnO	0.06	0.07	0.04	0.06	0.04	0.23	0.08	0.03	0.03	0.03	0.03	0.07	0.03	0.03	0.16
MgO	0.34	1.43	0.40	1.58	3.15	4.67	2.10	1.08	0.79	0.77	0.15	0.15	0.19	0.61	19.2
CaO	1.52	1.77	1.39	3.45	5.71	6.33	3.30	2.65	1.61	2.08	0.19	0.66	0.18	1.01	6.74
Na_2O	2.34	3.05	1.97	2.64	3.33	3.36	2.81	2.69	2.53	2.76	3.21	2.23	2.91	2.23	0.98
K_2O	5.79	4.26	6.36	3.25	1.08	1.56	3.40	4.63	5.22	5.00	6.33	5.95	5.87	5.26	0.88
P_2O_5	0.09	0.41	0.17	0.17	0.51	0.91	0.17	0.24	0.17	0.17	0.07	0.06	0.07	0.25	0.10
Orig. Sum	98.4	100.5	100.7	101.5	101.5	96.3	100.1	100.8	97.7	100.6	103.3	99.2	102.7	102.0	98.0
ppm															
Sc	7.2	17.7	9.4	19.5	26.6	27.4	18.2	14.1	4.9	12.9	4.1	3.8	2.8	8.9	9.0
Cr	4	33	3	26	56	153	51	24	8	19	2	3	3	6	118
Co	2.1	11.7	4.5	11.5	22.7	33.8	15.2	9.5	5.2	7.5	0.7	1.1	0.9	-	74.9
Ni	-	-	20	30	-	-	30	30	10	10	3	-	7	15	80
Rb	203	231	202	96	17	75	100	205	252	189	165	169	206	147	72
Cs	0.39	0.72	0.14	0.23	-	0.57	0.14	1.29	0.45	0.83	0.16	0.19	0.17	0.69	1.30
Sr	140	510	220	430	450	220	290	210	170	90	-	100	40	90	390
Ba	960	900	900	1580	390	600	760	1170	890	750	280	460	800	920	320
La	51.6	66.0	39.6	88.2	49.2	27.3	42.5	56.3	41.9	60.2	10.4	19.0	27.0	38.9	10.6
Ce	96.4	91.1	69.0	179	114	61.0	85.0	117	77.8	123	17.2	31.6	51.5	51.0	17.3
Nd	41	67	31	82	62	31	42	50	31	54	5	10	15	9	9
Sm	7.56	15.9	6.88	16.9	13.0	6.61	8.99	9.51	6.25	11.1	0.94	2.93	3.55	1.59	2.39
Eu	1.55	3.07	3.07	4.02	2.52	2.24	1.80	2.11	1.39	1.48	0.29	0.38	1.11	1.58	0.96
Tb	1.27	2.14	0.96	1.66	1.93	0.97	1.26	1.37	0.90	1.49	0.25	1.16	0.35	0.20	0.52
Yb	4.21	5.20	2.70	4.03	5.36	2.61	4.38	3.67	1.86	3.50	2.30	7.51	0.87	1.48	1.63
Lu	0.60	0.71	0.42	0.60	0.80	0.37	0.68	0.48	0.27	0.43	0.30	1.08	0.16	0.15	0.24
Zr	170	230	500	540	170	140	210	350	200	290	40	40	220	340	40
Hf	8.8	9.6	23.8	25.4	5.3	4.7	9.4	10.8	6.7	9.9	1.4	2.2	7.9	15.0	1.0
Ta	0.90	1.20	0.50	1.90	2.10	0.85	0.67	0.84	0.40	0.79	0.10	0.35	0.15	-	0.29
Th	0.2	0.5	0.1	3.4	1.1	0.2	0.2	2.8	0.5	4.8	0.5	0.9	9.1	3.5	4.5
U	-	0.9	-	1.4	-	-	-	0.8	0.4	1.1	0.6	0.8	4.9	2.4	1.3

[1]Reference for major element data: (1) Hudson, 1981; (2) Sinha and Bartholomew, 1984; (3) previously unpublished data.
*Total Fe as FeO; Rb and Sr values in boldface print from Pettingill et al., 1984.

(White and Chappell, 1977) or even C-type sources (Kilpatrick and Ellis, 1992). The wide range in A/CNK, up to ~1.3, generally follows SiO_2 abundance and probably reflects a mixed protolith of relatively unaltered volcaniclastics and reworked quartz-enriched sediments. High SiO_2 BH and QF gneisses overlap the lower-SiO_2 range of NGG, two samples of which represent the low end of the overall range in SiO_2 for the Pedlar massif. Except for a few PRCS outliers, TiO_2, FeO, CaO, K_2O and P_2O_5 abundances produce identical trends among the various groups. Variations in K_2O, TiO_2 and P_2O_5 vs. SiO_2, and the AFM diagram of Pedlar rocks by Bartholomew et al. (1991), are nearly identical to those of C-type magmatic charnockites of Kilpatrick and Ellis (1992).

Chemical dispersion associated with mafic and felsic layers, especially in MgO and K_2O, is depicted by tie-lines shown for the 115A–115C pair and by other samples lying off the overall

Table 4
Geochemical sample locations on U.S. Geological Survey 1:24 000-scale 7.5-minute quadrangle maps

Sample	7.5′ Quad.	Longitude	Latitude	Sample	7.5′ Quad.	Longitude	Latitude
Pedlar River Charnockite Suite				Vesuvius Megacrystic Charnockite			
B-56	Sherando	78°58′22″	37°54′12″	167M	Montebello	79°08′47″	37°51′58″
180-GVR	Montebello	79°12′44″	37°47′17″	B-37	Vesuvius	79°10′27″	37°53′17″
BR-273	Montebello	79°07′49″	37°47′35″	H-56	Vesuvius	79°09′24″	37°52′39″
BR-96	Massies Mill	79°06′39″	37°47′04″				
HP-25	Massies Mill	79°06′23″	37°47′14″	Nellysford Granulite Gneiss			
HP-26	Massies Mill	79°06′20″	37°47′14″	178NC	Montebello	79°12′35″	37°48′34″
HP-27	Massies Mill	79°06′26″	37°47′15″	179-GVR	Montebello	79°12′54″	37°47′36″
HP-29	Montebello	79°09′48″	37°47′00″	188-NCR	Montebello	79°12′52″	37°48′33″
HP-33	Montebello	79°13′52″	37°46′18″	196	Sherando	78°53′56″	37°53′39″
P-3R	Montebello	79°10′01″	37°49′48″	215B	Sherando	78°52′43″	37°57′32″
P-4R	Montebello	79°10′32″	37°49′09″	236A	Sherando	78°54′16″	37°54′11″
199	Greenfield	78°52′41″	37°57′53″	B-105A	Greenfield	78°50′14″	37°57′44″
B-57	Sherando	78°59′37″	37°53′37″	B-108	Greenfield	78°50′18″	37°57′47″
212A	Sherando	78°52′38″	37°57′33″	B-54	Greenfield	78°50′09″	37°57′47″
B-64	Sherando	78°58′15″	37°54′14″	B-82	Sherando	78°53′51″	37°54′02″
HP-31	Montebello	78°11′15″	37°47′01″				
P-7R	Montebello	79°12′11″	37°47′39″	Biotite-hypersthene Granulite Gneiss			
172M	Montebello	79°08′17″	37°52′14″	185-IC	Montebello	79°14′03″	37°49′25″
B-130	Greenfield	78°51′27″	37°57′40″	186-PRR	Montebello	79°14′07″	37°47′35″
S-2	Montebello	79°13′52″	37°46′18″	90-IC	Montebello	79°13′30″	37°49′20″
115A	Sherando	78°56′47″	37°54′22″				
115C	Sherando	78°56′47″	37°54′22″	Quartzofeldspathic Gneiss			
435	Greenfield	78°50′22″	37°58′57″	136-NC	Montebello	79°12′24″	37°48′39″
218	Greenfield	78°51′29″	37°57′44″	121	Sherando	78°55′38″	37°54′34″
141	Sherando	78°55′15″	37°53′30″	173M	Montebello	79°08′02″	37°52′01″
447	Greenfield	78°51′01″	37°57′01″	BR-39	Buena Vista	79°16′16″	37°44′52″
89IC-1	Montebello	79°13′32″	37°49′22″	Norite			
				344A	Greenfield	78°51′32″	37°57′49″

trends. Major element variations yield three principal groups readily apparent on the QAP diagram (Fig. 4). The main group of Pedlar compositions lies within the farsundite sub-field of charnockites (orthopyroxene-bearing monzogranite), and follows a rough trend toward a more plagioclase-rich group comprising small clusters in the fields of charno-enderbite (orthopyroxene-bearing granodiorite), quartz-bearing jotunite and jotunite (monzodiorite). Variants in the PRCS that fall off the general trends in Figs. 3 and 4 include four leucocratic samples, three of which are layered charnockites (115C, 447 and 218), plus one massive sample (B-130), which represent compositionally distinct charnockitic bodies. Within the plagioclase-rich group of compositions in Fig. 4, three PRCS and one VMC sample form a small cluster in the quartz jotunite field that exhibits a chemical dispersion parallel to that produced by the banded rocks (e.g. 115A-C). Similar chemical dispersion is apparent for the cluster of three NGG and one PRCS jotunites closer to the plagioclase apex, as well as a single mangerite (56) offset from the main group.

3.2. Trace elements

Trace element signatures of three representative Pedlar charnockites (Fig. 5) exhibit significant departure from bulk, lower and upper continental crustal signatures (Taylor and McLennan, 1985, 1995). Relative to average continental crust, PRCS units are systematically higher in incompatible large ion lithophile elements (LILE) Rb, Ba, K; light rare earth elements (LREE) La, Ce, Nd and Sm; as well as more compatible Zr and Hf. This

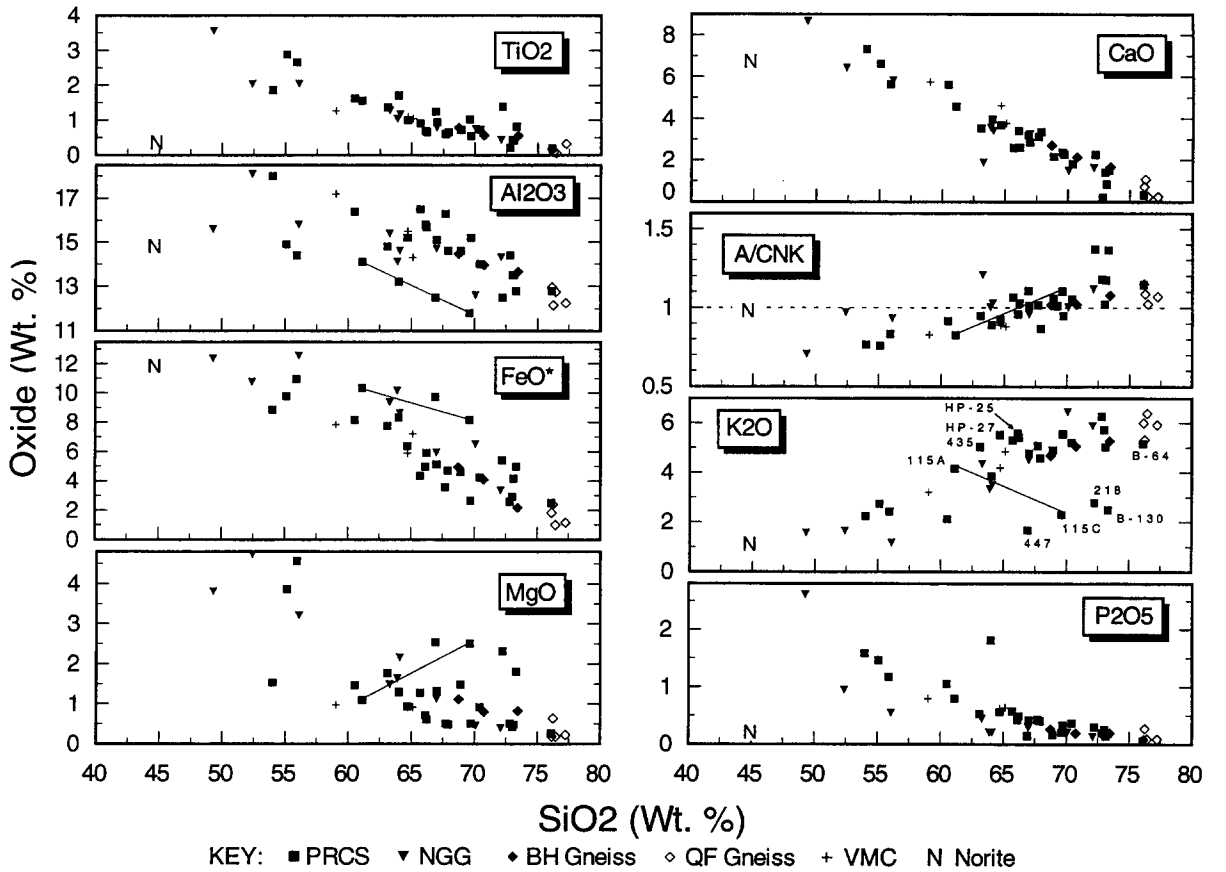


Fig. 3. Harker diagrams of major oxides and A/CNK ratios (molar $Al_2O_3/[CaO+Na_2O+K_2O]$) in rocks from the central Pedlar massif. Solid tie-lines are shown in several diagrams for a pair of compositionally banded charnockite samples representing melanosome (115A) and leucosome (115C). Abbreviations for units are: PRCS = Pedlar River Charnockite Suite, VMC = Vesuvius megacrystic charnockite, NGG = Nellysford granulite gneiss, BH = biotite–hypersthene gneiss, QF = quartzofeldspathic gneiss, and N = norite.

enrichment yields a regular pattern, reflecting increasing compatibility from Rb to Lu in the series and significant differentiation involving crystal–liquid segregation and/or assimilation. Much of this enrichment likely occurred during initial magmatic episodes that produced the PRCS protolith. Less enrichment is evident for Ta, Sr, P and the heavy rare earth elements (HREE) Tb, Yb and Lu; while Cs, Th, Ti and Sc are significantly depleted relative to continental crust. Negative anomalies for mildly compatible Ta (similar to Nb), Sr, P and HREE; and strongly compatible Ti and Sc are observed in C-type compositions (Kilpatrick and Ellis, 1992) which argues in favor of a magmatic petrogenesis of the PRCS.

Dispersions in trace LILE across general trends are much greater than those in major elements as evident in plots of Rb, Ba, La and Th relative to SiO_2 (Fig. 6). Except for a few outliers, overall trends in PRCS rocks indicate a predictive increase in Rb with SiO_2, whereas Ba decreases and La shows no apparent trend. Abundances of Th randomly vary by nearly three orders of magnitude; the highest values of Th (~10–80 ppm) in some charnockites are possibly complementary to depleted Th signatures in others (Fig. 5), but show no relation to SiO_2 content. These gross variations might be explained by trace element distribution (e.g. Nash and Crecraft, 1985) inherent in magmas which were involved in evolution of the volcanic

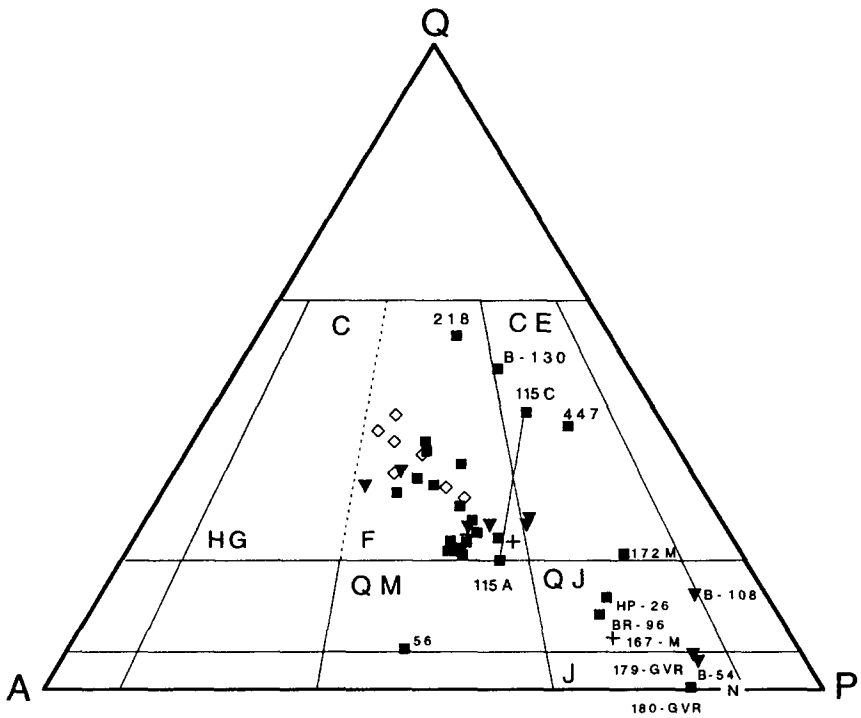


Fig. 4. Quartz-alkali feldspar-plagioclase (QAP) ternary diagram for central Pedlar massif normative compositions. Tie-line is shown for the 115A–C compositionally layered pair of charnockites suggesting that similar parallel trends exist between the main grouping of Pedlar rocks and several high-Q outliers. Abbreviations for classification fields from Streckeisen (1974), Streckeisen (1976) are: C = charnockite, HG = hypersthene granite, F = farsundite, CE = charnoenderbite, QM = quartz mangerite, QJ = quartz jotunite, and J = jotunite. Symbols are the same as in Fig. 3.

protolith. Decrease in Ba with igneous differentiation follows the CaO trend (Fig. 3) due to ubiquitous plagioclase fractionation. Incompatible Rb follows the K_2O trend of increasing abundances with SiO_2 typical of calc-alkaline volcanic series (Gill, 1981). However, dispersion across these trends suggests that much of the variation is related to effects of element partitioning associated with partial anatexis and melt segregation during granulite facies metamorphism. Plagioclase-rich zones are enriched in Ba and depleted in Rb relative to zones with higher proportions of alkali feldspar, quartz and biotite. This is exemplified by the regions outlined for BH and QF granulite gneisses in Fig. 6, the most silicic compositions of the Pedlar massif. The lack of any definitive trends in La is possibly due to ubiquitous occurrences of REE-rich accessory minerals and major minerals that are variably REE-compatible. Recent experimental studies (Watt and Harley, 1993; Beard et al., 1994) indicate a profound influence by accessory mineral solubilities on the geochemistry of granulite-facies melts and residual rocks.

Notable variations in Sm/Yb vs. Hf/Ta (Fig. 7A) and Ta vs. Hf (Fig. 7B) occur in many Pedlar rocks, but the Pedlar massif displays significant increases in both of these ratios over average continental crustal ratios. The chemical variation, such as the range in Hf from ~ 1.4 to 34 ppm, probably reflects high partition coefficients in high field strength elements (HFSE) Hf and Ta and HREE in garnet and ferromagnesian minerals, especially Fe–Ti oxides, and low partition coefficients in quartz and feldspars (Nash and Crecraft, 1985). Leucocratic members, such as the QF gneisses and some PRCS samples, typically

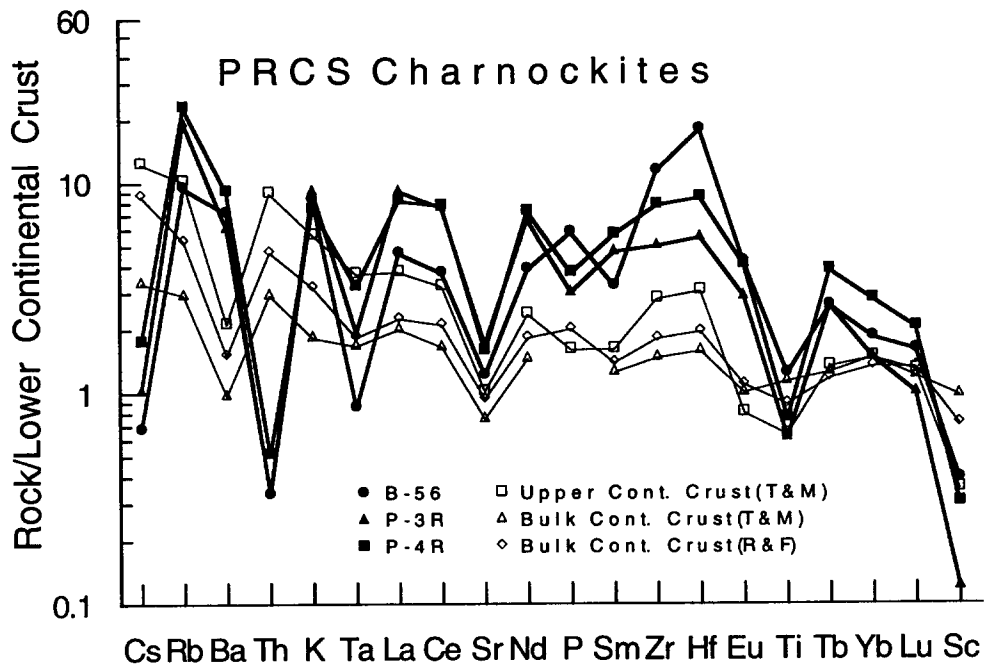


Fig. 5. Chemical patterns for typical PRCS charnockites and average compositions of the upper continental crust and bulk continental crust normalized to lower crustal composition of Rudnick and Fountain (1995). The element sequence corresponds to increasing compatibility in lower crust and mantle regimes. Average crustal abundances are from (Taylor and McLennan, 1985, Taylor and McLennan, 1995) and (Rudnick and Fountain, 1995).

have low abundances of Hf and Ta, whereas increasing amounts of these elements are present in mafic samples. Relative proportions of Hf- and Ta-compatible minerals, especially insoluble accessory minerals such as zircon and sphene are likely controlling factors during partial melting, especially since these elements directly replace stoichiometric elements (Hf for Zr, Ta for Ti) in the crystal lattices. Therefore, it is reasonable to assume that compositions with relatively high Ta and Hf are enriched in sphene and zircon, respectively, and represent either heterogeneity of sampled material or restite zones where these minerals were concentrated during melt segregation.

Similar processes are apparent for some transition metals in which Co and Cr generally increase with Sc along a possible protolith trend (Fig. 8), with the highest values being found in the NGG units. Effects of major or accessory minerals in restite are greater on Cr, which ranges from 2.5 to 135 ppm in the PRCS, than on Co for which dispersion is not appreciable. An approximately 15 × separation of Cr occurs in the 115A–C sample pair (7 vs. 107 ppm) and a significant increase in Cr occurs in both high- and low-SiO_2 units that are enriched in MgO, depleted in K_2O, and either lie off the main PRCS trend or close to the plagioclase apex on the QAP diagram (Fig. 4). Higher Cr in the leucocratic PRCS rocks (115C, 218, 447 and B-130) and in NGG samples such as B-54 (Fig. 8) is either related to formation of accessory Mg–Cr garnet by dehydration–melting reactions involving peraluminous protolith compositions (e.g. Patiño Douce and Johnston, 1991) or represents heterogeneity in protolith material due to presence of a Cr-bearing mineral such as spinel or garnet. The occurrence of Cr disparity particularly in the 115A–C pair and other layered charnockites indicates that Cr abundances are directly related to the formation of mineralogic banding.

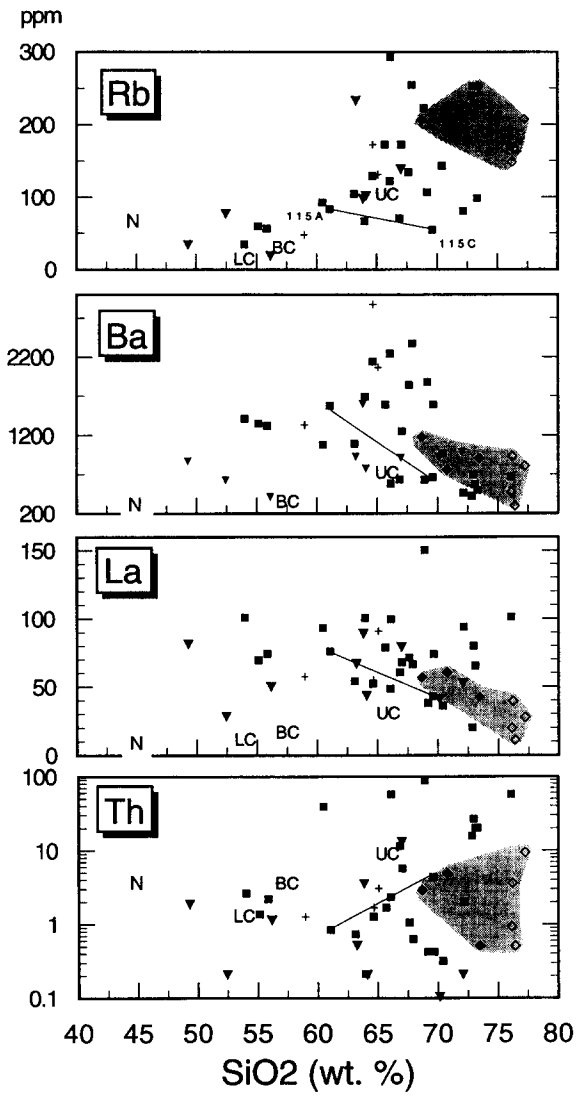


Fig. 6. Selected LILE variations relative to SiO_2 in the Pedlar massif illustrate diversified controls on trace elements depending on chemical behavior during granulite facies metamorphism. Tie-lines for 115A–C layered pair indicate possible ranges and directions of chemical dispersion from overall protolith trends of incompatible/soluble Rb, feldspar-compatible Ba, slightly compatible La and incompatible/insoluble Th with increasing SiO_2. Shaded fields delineate high-SiO_2 BH and QF gneisses. Abbreviations for continental crustal compositions are the same as in Fig. 5. Symbols are the same as in Fig. 3.

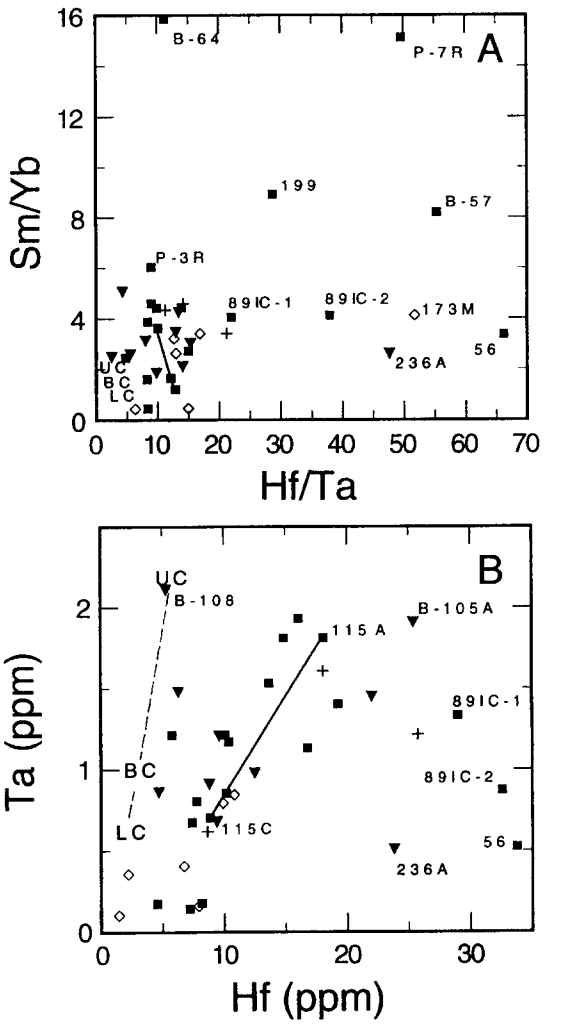


Fig. 7. Variations in (A) Sm/Yb relative to Hf/Ta ratios, and (B) Ta relative to Hf abundances in the central Pedlar massif. Moderate variations in Sm/Yb ratios in most units are exceeded by more extensive increases in the Sm/Yb of variant PRCS members B-64, P-7R, 199, and B-57. Relatively high Hf/Ta ratios in several units do not correlate with Ta and Hf abundances which are dispersed by dehydration melt segregations involving Ta- and Hf-compatible accessory minerals. Abbreviations for continental crustal compositions are the same as in Fig. 5. Symbols are the same as in Fig. 3.

3.3. REE in charnockites

Chondrite-normalized rare earth element patterns of typical PRCS rocks (Fig. 9A) are LREE-enriched and grossly monotonic over the REE

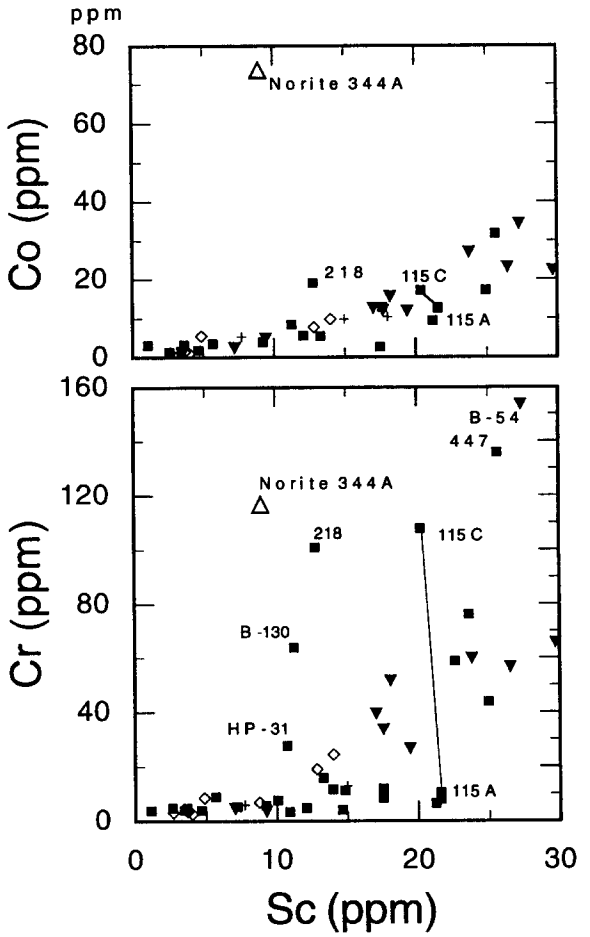


Fig. 8. Co and Cr vs. Sc in Pedlar rocks suggest greater stability of Co during formation of compositional layers relative to much wider variation in Cr, as depicted by the 115A (melanosome)–115C (leucosome) layered pair of charnockites. Higher Cr values in SiO_2-rich rocks correspond to crystallization of Mg–Al garnet during melt segregation. Symbols are the same as in Fig. 3.

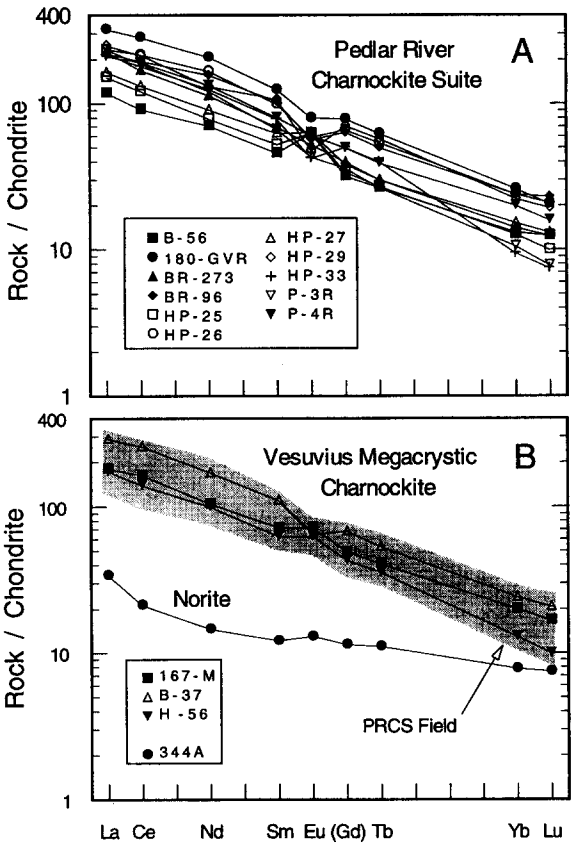


Fig. 9. Chondrite-normalized REE patterns of typical units in (A) the Pedlar River Charnockite Suite (PRCS), and (B) the Vesuvius megacrystic charnockite (a coarse-grained equivalent of the Pedlar charnockites) and a norite within the PRCS. The single norite sample is shown for comparison; however, its relation to the charnockites within the Pedlar massif is questionable. Chondrite normalization values are calculated volatile-free abundances from Anders and Ebihara (1982).

series, except for slight positive or negative complementary Eu anomalies. Light REE range from ~100 to 300 × chondritic values, whereas Yb and Lu range from ~7 to 21 ×, yielding a uniform three-fold range in REE without significant fractionation. Involvement of REE-rich accessory phases such as zircon and apatite, as well as the granulite minerals garnet and pyroxene, would exhibit significant LREE/HREE fractionation (e.g. Fujimaki, 1986; Fujimaki et al., 1984); thus the range is most likely inherited from the PRCS protolith and not due to subsequent fractionation. Vesuvius megacrystic charnockite samples (Fig. 9B) fall in the upper part of the normal PRCS range, but are otherwise very similar to the normal PRCS.

On the contrary, the norite sample 344A (Fig. 9B) has lower overall REE and a less fractionated HREE pattern compared to the PRCS. Although involvement of the norite in the petrogenesis of charnockites is possible, any relation other than as a mafic melt that intruded the

granulitic massif is obscure. A consanguineous relation between the norite and PRCS rocks is not supported by other chemical signatures (Figs. 3, 6 and 8).

Compositionally layered PRCS members (Fig. 10A) exhibit complementary REE patterns as shown by the 115A–C pair. Compared to normal PRCS, layered samples with a higher proportion of mafic minerals have high total REE and slight negative Eu anomalies, in contrast to felsic samples which have low total REE, and a pattern characterized by depleted middle REE and a positive HREE slope. Felsic samples 141 and 115C also contain higher SiO_2 (~70 wt.%) relative to average PRCS further indicating an inverse relation between SiO_2 and total REE contents due to REE incompatibility with quartz. The slightly enriched HREE patterns in samples 141 and 115C cannot be related to zircon because there is no concomitant increase in Zr abundance. Actually, the highest Zr abundances in the PRCS suite occur in samples 89IC-1 and 89IC-2 (Fig. 10A) which display complementary REE patterns. Two other layered samples, 218 and 435 (Fig. 10B), have overall REE abundances similar to those of the normal PRCS group, albeit with elevated HREE signatures and more pronounced negative Eu anomalies. Their REE signatures are most likely related to slightly higher than normal amounts of HREE-compatible garnet and/or lower amounts of apatite which is highly compatible to REE, especially the middle REE. Enhanced garnet involvement is further supported by high MgO and Cr in sample 218, and moderate to high MgO and Cr in sample 435 which shows less HREE enrichment. The effects of apatite are difficult to evaluate due to the lack of significant association of chemical variations with P_2O_5 and CaO abundances.

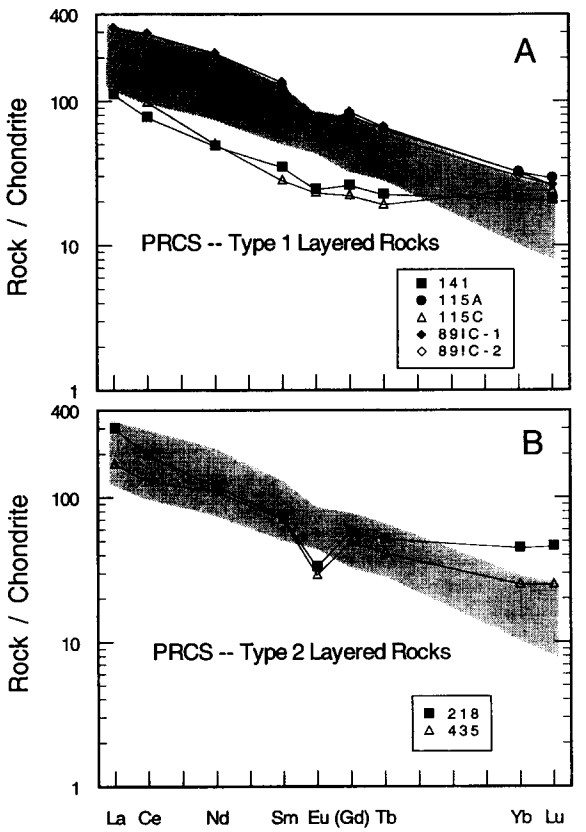


Fig. 10. Chondrite-normalized REE patterns of PRCS samples having known field relations and/or textures representing compositionally banded leucosomes and melanosomes. (A) Type 1 layered rocks are exemplified by the 115A–115C sample pair collected at one outcrop, while other samples are indirectly associated by texture and chemical signature. (B) Type 2 layered rocks reflect plagioclase fractionation to yield a negative Eu anomaly, and crystallization of garnet or other HREE compatible phase. (same parameters as Fig. 9)

3.4. REE and Th in PRCS variants

High-Th variants of the PRCS, divided into REE varieties without Eu anomalies (Fig. 11A) and those with negative Eu anomalies (Fig. 11B), generally have much steeper REE patterns and higher SiO_2 contents (except for 447 and 172M), and Th concentrations ranging from ~10 to 83 ppm. PRCS variants without Eu anomalies (samples 447, 199, B-57 and 172M) represent four unrelated units as depicted in their mismatched REE signatures. Of these four, 172M is the only one with a REE pattern and overall chemistry characteristic of the PRCS. The REE pattern of layered sample 447 strongly supports the involvement of Mg garnet noted above. High-Th variants with negative Eu anomalies (Fig. 11B) exhibit steepened REE patterns in which La ranges from ~100 to 1800 × chondritic value, with normalized La_N/Lu_N ratios of ~100 compared to La_N/Lu_N

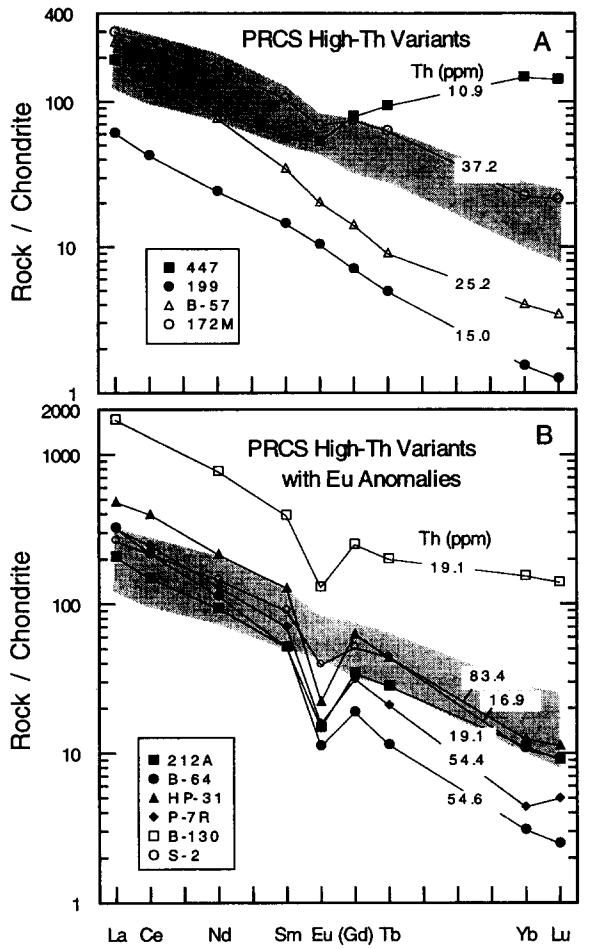


Fig. 11. REE patterns of high-Th variants indicate association between elevated Th and REE divergence within the Pedlar River Charnockite Suite. (A) High-Th variants without Eu anomalies are significantly different from each other indicating variable petrogenetic processes involving Th-rich accessory phases. Samples B-57 and 199 (two lower patterns) are high-SiO_2 varieties dominated by REE-poor quartz and feldspar, whereas sample 447 indicates crystallization of HREE-compatible garnet. (B) High-Th variants with negative Eu anomalies have distinctly steeper REE slopes relative to normal PRCS representatives and represent liquids segregated during granulite facies dehydration melting. Models suggest their derivation as low-degree partial melts from typical PRCS sources leaving restitic plagioclase, K-feldspar, and pyroxenes ± garnet. (same parameters as Fig. 9)

~12–15 in the PRCS. Occurrence of Th-rich members within the PRCS provides a complement to Th-depleted members and diminishes any requirement for a Th-depleted protolith.

The lack of any systematic REE–Th relations in Fig. 11 suggests that the mechansim responsible for Th enrichment is independent of REE divergence from the normal REE pattern in the PRCS, although the two processes are concomitant. Wide variations in Th possibly reflect inhomogeneous distribution of Th-rich accessory minerals such as apatite, sphene and monazite; however these minerals are poor candidates because P and Ti do not correlate with Th (Table 1). Otherwise the REE patterns are similar to the Type 2 leucogneisses of Watt and Harley (1993) which exhibit strong enrichment in Th due to accessory mineral entrainment.

3.5. *REE in granulite gneisses*

Rare earth element patterns of NGG samples (Fig. 12A) are essentially identical to those of normal PRCS although with a slightly wider range in abundances of light and middle REE. Minor differences cannot be deemed significant in light of the wide range of major and trace element abundances in the Pedlar massif. There are no means to chemically distinguish between normal PRCS and NGG because other elemental data show similar ranges and considerable overlap.

Conversely, QF and BH gneisses (Fig. 12B) exhibit a wide range in REE patterns that reflects variable LILE depletion and concomitant SiO_2 enrichment, the effects of which increase from BH to QF types. BH gneisses have REE signatures similar to those of the normal PRCS and thus are not extensively depleted, but like the NGG, the members having the lowest values extend slightly beyond the lower limit of normal PRCS. In this respect, the BH gneisses are essentially identical in major and trace element abundances to the most REE-depleted NGG, whereas QF gneisses are overall chemically similar to higher-SiO_2 felsic PRCS layers implying a comparable petrogenesis.

4. REE models and constraints on petrogenesis

Relative proportions of essential minerals in the PRCS are likely responsible for minor changes in overall REE abundances and relatively insignificant

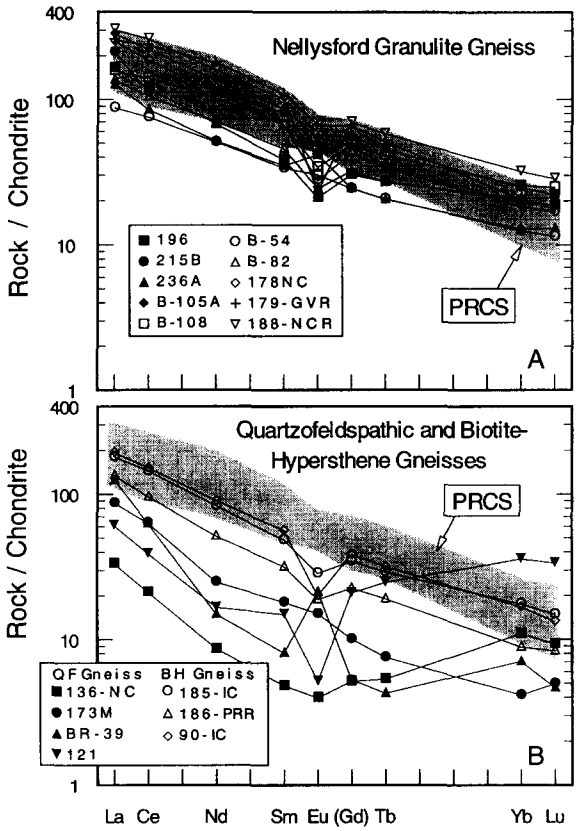


Fig. 12. REE patterns of granulite gneisses in the central Pedlar massif. (A) Nellysford granulite gneiss REE are essentially equivalent to PRCS and do not show the effects of compositional segregation except for marginally wider separation in REE abundances. (B) Biotite–hypersthene (BH) gneisses (open symbols), representatives of the Lady Slipper Granulite Gneiss, are similar to the lowest PRCS, but with more pronounced negative Eu anomalies reflecting higher quartz and complementary association with plagioclase-rich units. Quartzofeldspathic (QF) gneisses are strongly depleted in overall REE. The variable Eu anomaly and heavy REE enrichment reflect non-uniform effects of garnet, plagioclase and pyroxene that crystallized from incipient melts. (Same parameters as Fig. 9.)

pattern fractionation. Positive Eu anomalies are apparent for low REE patterns, whereas negative Eu anomalies prevail in samples with higher REE in the series, so the overall variation is related to the proportions of Eu-compatible plagioclase and REE-incompatible quartz. Significant fractionation of LREE/HREE would indicate involvement of REE-compatible accessory phases such as garnet, apatite, zircon, monazite and possibly pyroxene having non-uniform REE partitioning during metamorphic recrystallization, incipient dehydration melting, or crystal–liquid fractionation. The latter process would probably ensue during mobilization or final emplacement of charnockitic magma.

Petrogenetic constraints on PRCS rocks follow assumptions that although absolute partition coefficients can vary widely in igneous systems, actual relative partition coefficients are not too divergent from typical reported values (e.g. Fujimaki et al., 1984; Nash and Crecraft, 1985; Fujimaki, 1986) and that accessory minerals involved in granitoid petrogenesis concentrate a large proportion of certain trace elements (e.g. Watt and Harley, 1993; Beard et al., 1994). Any significant departure of trace element signatures from the normal PRCS pattern must have involved some combination of: (1) low-degree melting in which fractionated liquids segregated from granulitic restite, and (2) disequilibrium melting in which phases rich in certain trace elements were entrained in the melt or concentrated in the residue. Detailed models of charnockite melting by Beard et al. (1994) which rely on partial REE analyses of apatite, zircon and monazite, provide a basis for comparing myriad compositions belonging to the PRCS. Using their models to interpret PRCS compositions, layered rocks (Fig. 10) indicate a separation of REE-compatible minerals such as pyroxenes and biotite from REE-incompatible felsic zones containing proportionately higher quartz + feldspars.

Depletion of middle REE yields bow-shaped patterns in melts that are possibly related to the effects of residual apatite which is highly compatible to middle REE. However, relative increase in the HREE in layered charnockites also can be explained by retainment of garnet in the residuum (Watt and Harley, 1993), while the negative Eu anomaly is due to separation of low-degree melts from restitic plagioclase and alkali feldspar. Derivation of the composition represented by sample 447, a PRCS high-Th variant highly enriched in HREE (Fig. 11A), requires either accumulation of an HREE-compatible phase, such as garnet or zircon (Fujimaki, 1986) or selective entrainment of such phases into disequilibrium

melts. The two other variants shown in Fig. 11A (199 and B-57) have higher SiO_2 (~73%), strongly depleted HREE signatures and overall low REE representing either restite having low bulk D_{REE} dominated by quartz and feldspar or leucogranitic melts segregated from plagioclase-free restite.

Steep REE patterns and pronounced negative Eu anomalies in high-Th PRCS variants (Fig. 11B) suggest derivation by magmatic fractionation in which low-degree melts separated from a granulitic restite. The compositions can be modeled by moderately low-degree (e.g. <10%) partial melting of the protolith leaving a restite mineralogy of pyroxene + plagioclase ± garnet ± zircon, but virtually devoid of LREE-compatible phases such as apatite and monazite. This process requires efficient melt segregation and depletion of LREE-compatible phases in the restite. From a model source with an average PRCS composition, a liquid derived by ~1–5% partial melting, leaving residual feldspars + pyroxenes ± garnet ± zircon, will exhibit the observed compositional range of the high-Th variants in the PRCS. Bulk distribution coefficients calculated for mineral–liquid partition coefficients appropriate for evolved silicic magmas (e.g. Nash and Crecraft, 1985) are $D_{Th}=0.09$, $D_{La}=0.63$, and $D_{Lu}=2.4$ for a residuum of plagioclase (40%) + K-feldspar (30%) + clinopyroxene (20%) + orthopyroxene (10%). Addition of garnet or zircon to the residuum increases partitioning of HREE into the residuum, thereby enhancing fractionation of the REE pattern. Addition of quartz to the residuum, which is stable throughout granulite melting (e.g. Patiño Douce and Johnston, 1991), further increases the REE concentration in the melt because of it low compatibility to all trace elements (Nash and Crecraft, 1985). Liquids derived by low-degree of melting are thus REE fractionated, enriched in Th, somewhat depleted in HREE, exhibit negative Eu anomalies, and have a steeper REE slope than the starting composition.

Variable Eu anomalies in BH and QF granulite gneiss (Fig. 12A) suggest fractionation due to plagioclase while positively sloping HREE patterns in QF gneisses 121, 136-NC and BR-39 indicate restitic HREE-compatible phases such as pyroxene and garnet as noted for Type 1 banded PRCS rocks. The positive Eu anomaly in sample BR-39 reflects a relatively high proportion of plagioclase, whereas sample 173M shows no effect of either plagioclase or HREE-compatible phase stabilization. Gross complementary relations in REE and other elements exist between the QF and BH gneisses further implying that these two units represent compositional segregations on a regional scale which is supported by their field association in Fig. 2.

5. Discussion

5.1. Comparison with lower crustal rocks

Although the negative Ta, Sr, P, Ti and Sc anomalies in Fig. 5 are not too different from typical calc-alkaline volcanic patterns, the LILE signature in typical PRCS charnockites shows little overall fractionation from bulk crustal values, and Cs and Th are severely depleted. Other PRCS members, as well as NGG, are either depleted in Th or have complementary enrichments in Th, consistent with a significant amount of Th and U scatter in C-type Ardery charnockites and C-type volcanics reported by Kilpatrick and Ellis (1992). Depletion of incompatible Cs in PRCS compositions is possibly related to aqueous fluid scavenging prior to the onset of granulite metamorphism. This is likely due to high solubility and large ionic size of Cs compared to Rb which is equally soluble, but more compatible in K-feldspars due to its smaller ionic radius. This follows the expectation of marked depletion of Cs and strong fractionation of Rb/Cs ratios even in amphibolite facies rocks (Heier, 1973).

Depletion in K and other LILE, especially Cs, Rb, Th and U are reported for many granulite facies terranes (e.g. Sighinolfi, 1971; Lambert and Heier, 1967; Heier, 1973; Condie and Allen, 1984; Rudnick et al., 1985). Some systems, such as the Musgrave Block granulites in Australia (Gray, 1977) do not exhibit overall LILE depletion, and some southern Indian granulites show LILE enrichment (Janardhan et al., 1983; Weaver and Tarney, 1983). Rudnick et al. (1985) reiterated commonly cited processes that could be responsible for LILE depletion during granulite metamor-

phism including: (1) separation of partial melt, and (2) fluxing of fluids without significant partial melting. Either process would depend greatly on the element partitioning effects of residual mineralogy, especially those related to trace element rich accessory minerals. The effects of accessory mineral instability will then be much greater on trace element signatures than on bulk chemistry.

Unlike individual LILE and REE signatures in banded gneisses and PRCS variants, REE patterns in Fig. 9A probably represent the protolith in a broad sense. Retainment of protolith signatures during granulite metamorphism has also been reported for Archean charnockites from India (e.g. Condie and Allen, 1984); however, extensive chemical changes related to dissolution of accessory minerals by carbonic fluids are noted for charnockites derived from gneisses in the Kabbalkdurga area (Stähle et al., 1987). The protolith of the PRCS is overall similar to average upper crust (Taylor and McLennan, 1985, 1995; Rudnick and Fountain, 1995) although the trace element signatures in Fig. 5 indicate some degree of crustal evolution typical of silicic volcanic systems.

5.2. *Interpretation of geochemical signatures*

Chemical variations outlined above require that the Pedlar massif experienced multiple and gradational processes related to a protracted Grenvillian metamorphic event spanning ~100–200 Ma. These include: (1) protolith chemical trends established from primary volcaniclastic and sedimentary series, (2) enhanced LILE mobility during amphibolite-to-granulite dehydration reactions, (3) incipient dehydration melting with either local segregation of melt and restite into leucosomes and melanosomes or en masse (melt + restite) mobilization and pluton emplacement, and (4) more extensive melting involving separation of magma from restite. Overall major and many trace element variations in Pedlar rocks are consistent with differentiation in a volcanic protolith although reworking by sedimentary processes might be responsible for SiO_2-enrichment in some samples, especially the four QF gneiss samples ($SiO_2 > 76$ wt.%) which exhibit strongly peraluminous compositions. Alternatively, SiO_2-enrichment could be related to feldspar and quartz accumulation from anatectic melts as suggested by Watt and Harley (1993) for cumulate leucogneisses from the Brattstrand Bluffs, Antarctica.

Explanation of the dominant Pedlar massif rocks involves at least two possible petrologic mechanisms, both of which are consistent with gross age relations. One hypothesis is that, during granulite facies dehydration melting, portions of deep-seated gneisses became locally mobilized as charnockitic (PRCS) plutons which subsequently intruded the overlying and surrounding (NGG and LSGG) granulite gneisses. In this scenario both lithologies would have been derived from a coeval protolith of volcanic and volcaniclastic units deposited before Grenvillian metamorphism. A second hypothesis is one in which pre-Grenvillian arc-generated plutons intruded comparatively shallow crustal sedimentary and volcaniclastic sequences, all of which were later subjected to Grenvillian granulite facies metamorphism. The latter scenario likely would have produced chemically different protoliths for PRCS and granulite gneisses because of two distinct episodes of magmatism; however, the general uniformity in major and trace element trends among charnockites and gneisses suggests a coeval relationship in support of the first hypothesis.

The NGG suite has several samples with anomalous Th and/or HFSE (178NC, 188-NCR, 236A and B-105A) which suggest involvement of accessory phases in melt/restite relations similar to those invoked for the PRCS. However, in terms of overall trace element signatures only minor petrogenetic differences exist between Nellysford granulite gneiss, normal charnockites and the Vesuvius megacrystic charnockite. Normal PRCS intrusions, including VMC units, are therefore interpreted as migmatitic plutons mobilized upward into NGG equivalent units and not subjected to extreme processes of LILE depletion from one region to the other. Higher P-T conditions of formation would be expected for the PRCS relative to NGG which were likely metamorphosed in shallower regions of the crust. This is supported by the younger radiometric ages for PRCS relative to NGG, but requires that LILE mobilization and/or melt segregation play a minimal role in the

NGG country rock. The similar trace element patterns of NGG and normal PRCS argue for a general lack of significant crystal/liquid fractionation due to either partial melt extraction or crystal accumulation.

Variable trace LILE enrichments and depletions that occurred during granulite facies metamorphism are evident in the disruption of overall protolith trends in PRCS layered rocks. The degree of this chemical dispersion must be high locally because many layers are found in large lenses and pods where physical segregation of leucosomes and melanosomes is of the order of several meters. The transition from amphibolite to granulite facies, with incipient dehydration melting, almost certainly involved mobilization of volatile incompatible LILE into migrating fluids, a process that resulted in gross depletions in Cs in the Pedlar massif. Petrogenesis of high-Th PRCS variants might, in some cases, involve the transport of Th by aqueous fluids during dehydration melting. This process would possibly enable greater heterogeneity of Th in the rocks affected by the metasomatizing fluids and, in part, serve as a mechanism to explain the large scatter in Th vs. SiO_2 (Fig. 5). However, evidence for such fluid transport has not been observed in any of the PRCS lithologies. Moreover, the mechanism would require concentrations far above the solubility limit (Harrison and Watson, 1983; Kay and Mahlburg Kay, 1986) thereby causing Th-rich minerals to stabilize and not yield Th-rich fluids.

Another likely process of chemical segregation is one demonstrated by Watt and Harley (1993) in which Rb, Ba, La and other LILE are retained by compatible restite phases that complement higher-SiO_2 melt compositions depleted in LILE. Pedlar rocks do not show significant overall depletion in Rb relative to K noted for other granulite terranes (e.g. Heier, 1973; Rudnick et al., 1985), perhaps because the protolith signature has not been affected as much. There is a tendency for decreasing Rb/K and Rb/Sr ratios with lower K content (Fig. 13) in the overall protolith trend, as well as significant metamorphic dispersion in Rb/K ratio at higher K content. However, dispersion in Rb/K ratio is not significant in the 115A–C sample

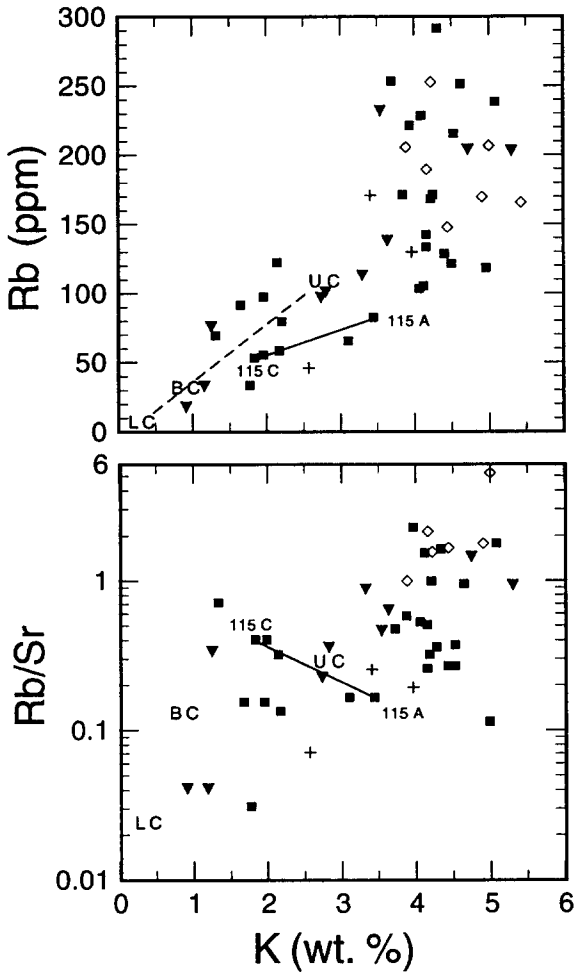


Fig. 13. Rb abundances and Rb/Sr ratios plotted against K in Pedlar massif compositions illustrate overall dispersion in LILE from the general trends and dramatic variation in Rb at high K contents. Tie-lines connect the 115A–115C layered pair of PRCS charnockites and indicate concomitant decrease in Rb and increasing Rb/Sr ratio with depletion of K. Abbreviations for continental crustal compositions (Taylor and McLennan, 1995) are the same as in Fig. 5. Symbols are the same as in Fig. 3.

pair indicating similar levels of depletion in K and Rb at lower K contents.

Increase in Rb/Sr ratios with K (Fig. 13) in the protolith is typical of differentiation series involving Sr-compatible plagioclase. Disruption across this trend is evident in the 115A–C pair, suggesting that Rb (and K) depletion in higher-SiO_2 units is

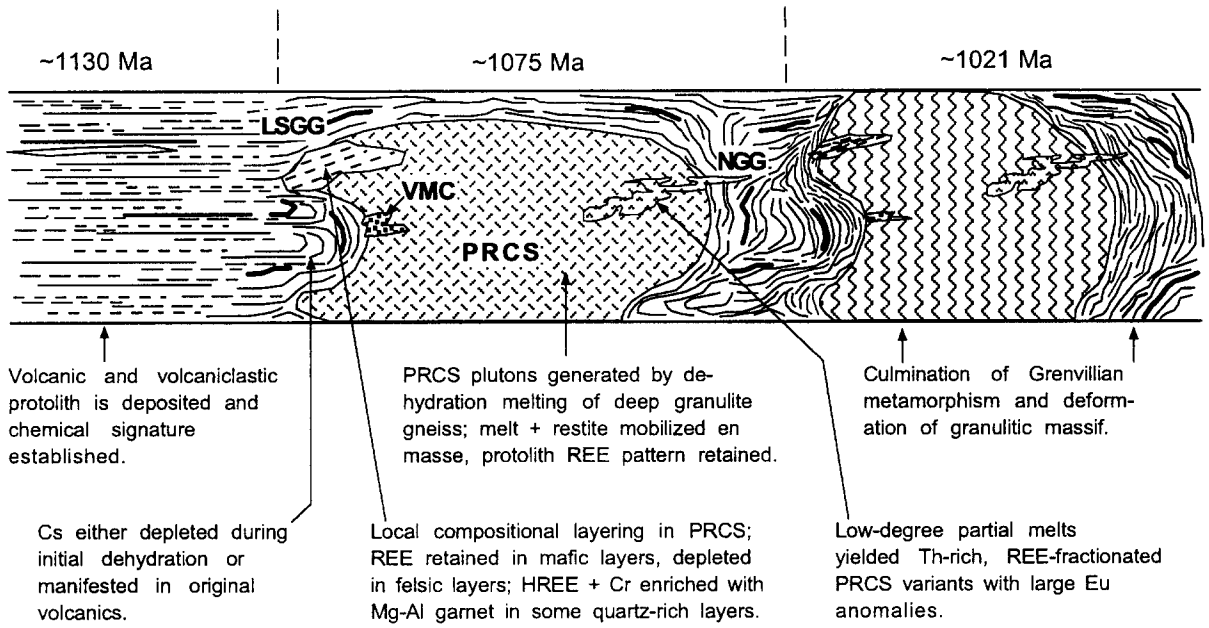


Fig. 14. Schematic showing petrogenetic mechanisms responsible for the major lithologic types occurring in the central Pedlar massif during the Grenvillian episode. Although protolith REE patterns are largely retained by the PRCS plutons, dispersions in K, Rb, Sr, Ba and Eu are produced by variations in feldspar and quartz proportions.

concomitant with increase in Rb/Sr ratio due to an even greater depletion of Sr. This is apparent in the drastic increase in normative quartz/feldspar ratio (Fig. 4) in felsic layers although relative to mafic layers the total felsic component is proportionately higher. Other trace elements are affected in a similar manner such that the more mafic layers yield higher overall LILE and REE signatures due to greater compatibility with mafic essential minerals and/or accessory phases. REE mobility thus appears to involve multiple mechanisms of aqueous and incipient melt fluids, but the nature of the metasomatic fluids would be difficult to determine without extensive studies involving phase equilibria, fluid inclusions, and isotopic signatures (e.g. Wickham, 1992).

The ~400% increase in Th between 115A and 115C is inconsistent with the depletion of other LILE shown by the tie-lines in Fig. 6. The nearly 10^3 variation in Th argues for processes other than LILE metasomatism or igneous differentiation that must also yield a petrogenetic decoupling from REE signatures. The highest Th values in charnockites are represented by PRCS variant compositions, four of which are accompanied by markedly higher Sm/Yb ratios and variable Hf/Ta ratios (B-64, P-7R, 199 and B-57) compared to the main cluster of samples shown in Fig. 7A which includes the 115A–C sample pair. This illustrates a correlation of Th mobility with changes in HREE and fractionation of HFSE Zr, Hf and Ta. Several Pedlar compositions experienced enhanced Hf/Ta ratios without concomitant steepening of the HREE slope. Most of these units have very low Th ($\leq$ ~0.4 ppm, e.g. samples 56, 89IC-1 and 236A) although one QF gneiss (173M) has relatively high Th (9.11 ppm). Such variations in insoluble elements cannot be related to mobility by aqueous fluid scavenging, but rather they suggest that incipient melts selectively entrained accessory phases such as apatite, monazite and zircon, or that such phases were made insoluble in the residuum. Conceivably, greater solubility of alkali elements (K, Rb, Cs) will likely result in a more ubiquitous depletion/enrichment controlled by essential minerals as demonstrated for other granu-

lite systems (e.g. Gray, 1977; Patiño Douce and Johnston, 1991). Less soluble Th, REE and HFSE will result in much greater local variation and a wider range in concentrations in regions affected by low-degree partial melting involving accessory phases.

Variable concentrations of Th more likely resulted from either melting out a Th-rich accessory mineral from the source region, or crystallization of such an accessory mineral from a Th+LREE-rich melt. Watt and Harley (1993) determined that the solubilities of zircon and monazite are very low under the water-undersaturated conditions of granulite partial melting. These minerals would most likely remain as accessory restite phases although monazite crystals smaller than 30 μm would be consumed in the melt. Monazite is not a ubiquitous accessory in Pedlar rocks, but it could occur as cryptic inclusions too small for petrographic detection. Melting of a Th-rich accessory during genesis of PRCS variant compositions, therefore, remains a possible mechanism of Th enrichment in some PRCS units. The overall REE patterns of high-Th PRCS variants suggest that they were derived as moderately low-degree partial melts that depleted the restite of any Th-rich accessory phases, but not HREE-compatible phases such as pyroxene, garnet or zircon. Other PRCS members and the granulite gneisses are more likely related to incipient dehydration melting involving only small-scale segregations of melt from restite.

Chemical variations among Pedlar granulites are thus the result of variable and combined processes ranging from incipient dehydration melting without a separate magmatic phase to partial melting which yielded a magmatic component. Petrologic mechanisms that we envision are responsible for derivation of the major lithologic type in the Pedlar massif are summarized (Fig. 14) as follows: The chemical signature of the protolith was established ($\sim$1130 Ma) during deposition of thick sequences of volcanic and volcaniclastic rocks. Relatively low abundances of mobile trace element Cs resulted either from depletion during initial dehydration of these layers from amphibolite to granulite facies, or the signature was inherent in the original volcanics. Early Grenville metamorphism ($\sim$1075 Ma) transformed these layers into granulite gneisses, while dehydration melting of deep-seated regions resulted in charnockitic plutons that were mobilized en masse into overlying NGG and LSGG. Small-scale liquid–restite segregations, perhaps in the transitional zone between gneiss and pluton, occurred locally to produce compositionally layered bodies that were incorporated into PRCS plutons. Low-degree melts within the charnockite plutons segregated into Th-rich, REE-fractionated variants of the PRCS. The entire massif of granulite gneisses and charnockites was extensively deformed during the culmination of Grenvillian metamorphism ($\sim$1021 Ma).

6. Conclusions

Granulite facies rocks belonging to the Grenvillian central Pedlar massif, represented by charnockites and granulite gneisses, span a compositional range of $\sim$47–79 wt.% SiO_2 and exhibit variable pervasive depletion of large-ion-lithophile elements (Rb, Ba, REE, etc.) with increasing silica content. Major and some trace element chemical trends indicate their origin from a mixed protolith of primary and reworked volcaniclastics. Chemical distinction between typical PRCS charnockites, the Vesuvius megacrystic charnockite and the Nellysford Granulite Gneisses cannot be made. We conclude that these rocks were derived from equivalent protoliths and that normal PRCS plutons represent mobilized portions of granulite gneiss undergoing incipient dehydration melting during granulite facies metamorphism.

Granulite facies chemical segregation, exemplified by the 115A–115C sample pair, is manifested in leucocratic layers of quartz, feldspar and garnet characterized by increased SiO_2, MgO, and Cr, with lower FeO, K_2O, REE, and other trace elements relative to the overall compositional trend. Field, petrologic and chemical data indicate formation of leucosomes by incipient dehydration melting involving restite dominated by REE-compatible pyroxenes and accessory apatite, along with other felsic phases and quartz. Strongly depleted quartzofeldspathic gneisses have REE patterns reflecting different amounts of HREE-compatible pyroxene and garnet, Eu-compatible

plagioclase, and REE-incompatible quartz stabilized in the residual mineralogy. They are thus believed to originate by processes nearly identical to those which formed PRCS layered members although SiO_2 enrichment and a tendency toward more peraluminous compositions by protolith weathering cannot be ruled out.

Highly depleted Cs values in the Pedlar massif reflect its solubility and incompatibility with any of the major mineral phases during either protolith evolution or amphibolite to granulite facies dehydration. Dispersions in K, Rb, Sr and Ba from the PRCS protolith signature are due to the relative proportions of major phases quartz, K-feldspar, plagioclase and biotite. Insoluble Zr, Hf, Ta and Th depend on partial melting and crystallization of accessory phases rich in trace elements, whereas Sc, Cr and REE mobility probably depends more on the proportions of minor minerals pyroxene and garnet (and plagioclase for Eu) involved in incipient melting or reaction during granulite facies dehydration.

Thorium abundances vary over three orders of magnitude, with extremely high Th abundances being associated with variant compositions in the typically Th-depleted Pedlar River Charnockite Suite. Four high-Th variants without Eu anomalies have mutually unrelated chemical signatures that resulted from different proportions of residual phases during dehydration melting. Six high-Th variants have light REE enrichment and HREE depletion resulting in steeper REE patterns and strongly negative Eu-anomalies. These charnockitic rocks represent low-degree partial melts ($\sim$1–5%) from normal PRCS or NGG protoliths to produce high-silica magmas capable of physical separation from the main charnockitic body.

Acknowledgements

Before their untimely deaths in 1985 and 1992, Dr Frank N. Abercrombie and Dr Robert J. Walker each analyzed many of the samples used in this paper. We regret that these former colleagues of the three senior authors were unable to share in the analysis of the data they helped obtain. Most of the trace element data were obtained under the auspices of the DOE Reactor User Sharing Program at The Radiation Center, Oregon State University. We thank former director A.G. Johnson and all other RC personnel for assistance in neutron irradiations and data acquisition. Arguments presented in this paper were significantly improved by thoughtful reviews by M. Raith and an anonymous reviewer. We also thank L. Corriveau and R.P. Tollo for provocative reviews of an earlier version of the manuscript.

References

Aleinikoff, J.N., Zartman, R.E., Walter, M., Rankin, D.W., Lyttle, P.T., Burton, W.C., 1995. U-Pb ages of metarhyolites of the Catoctin and Mount Rogers Formations, central and sourthern Appalachian: Evidence for two pulses of Iapetan rifting. Am. J. Sci. 295, 428–454.

Ames, R.M., 1981. Geochemistry of the Grenville basement rocks from the Roseland district, Virginia. Unpublished M.S. Thesis, University of Georgia, Athens, 91 pp.

Anders, E., Ebihara, M., 1982. Solar-system abundances of the elements. Geochim. Cosmochim. Acta 46, 2360–2380.

Badger, R.L., Sinha, A.K., 1988. Age and Sr isotopic signature of the Catoctin volcanic province: Implications for subcrustal mantle evolution. Geology 16, 692–695.

Bailey, C.M., Simpson, C., 1993. Extensional and contractional deformation in the Blue Ridge Province. Virginia. Geol. Soc. Am. Bull. 105, 411–422.

Bartholomew, M.J., 1977. Geology of the Greenfield and Sherando quadrangles, Virginia, VA. Div. Min. Resources, Publ. 1, 43 pp.

Bartholomew, M.J., 1981. Geology of the Roanoke and Stewartsville quadrangles, Virginia, VA. Div. Min. Resources, Publ. 4, 23 pp.

Bartholomew, M.J., Lewis, S.E., 1984. Evolution of Grenville massifs in the Blue Ridge geologic province, southern and central Appalachians. In: M.J. Bartholomew, E.R. Force, A.K. Sinha, N. Herz (Eds.), The Grenville Event in the Appalachians and Related Topics. Geological Society of America Special Paper, 194: 229–254.

Bartholomew, M.J., Lewis, S.E., 1992. Appalachian Grenville massifs: Pre-Appalachian translational tectonics. In: R. Mason (Ed.), Basement Tectonics, 7: 363–374

Bartholomew, M.J., Gathright II, T.M., Henika, W.S., 1981. A tectonic model for the Blue Ridge in central Virginia. Am. J. Sci. 281, 1164–1183.

Bartholomew, M.J., Lewis, S.E., Hughes, S.S., Badger, R.L., Sinha, A.K., 1991. Tectonic history of the Blue Ridge basement and its cover, central Virginia. In: A. Schulz, E. Compton-Gooding (Eds.), Geologic Evolution of the Eastern United States, Field Trip Guidebook, NE-SE GSA 1991. VMNH Guidebook, 2: 57–90.

Beard, J.S., Lofgren, G.E., Sinha, A.K., Tollo, R.P., 1994. Partial melting of apatite-bearing charnockite, granulite, and diorite:Melt compositions, restite mineralogy, and petrologic implications. J. Geophys. Res. 99 (B11), 21591–21621.

Bohlen, S.R., Mezger, K., 1989. Origin of granulite terranes and the formation of the lowermost continental crust. Science 244, 326–329.

Condie, K.C., Allen, P., 1984. Origin of Archaean charnockites from southern India. In: A. Kröner, G.N. Hanson, A.M. Goodwin (Eds.), Archaean Geochemistry. Springer, Berlin, pp. 182–203.

Elliot, W.C., Aronson, J.L., 1987. Alleghanian episode of K-bentonite illitization in the southern Appalachian basin. Geology 15, 735–739.

Evans, M.A., 1989. The structural geometry and evolution of foreland thrust systems, northern Virginia. Geol. Soc. Am. Bull. 101, 339–354.

Evans, N.H., 1991. Latest Precambrian to Ordovician metamorphism in the Virginia Blue Ridge: Origin of the contrasting Lovingston and Pedlar basement terranes. Am. J. Sci. 291, 425–452.

Fujimaki, H., 1986. Partition coefficients of Hf, Zr, and REE between zircon, apatite, and liquid. Contrib. Min. Petrol. 94, 42–45.

Fujimaki, H., Tatsumoto, M., Aoki, K., 1984. Partition coefficients of Hf, Zr, and REE between phenocrysts and groundmasses. J. Geophys. Res. 89, B662–B672.

Gill, J.B., 1981. Orogenic Andesites and Plate Tectonics. Springer, Berlin, 392 pp.

Gray, C.M., 1977. The geochemistry of central Australian granulites in relation to the chemical and isotopic effects of granulite facies metamorphism. Contrib. Min. Petrol. 65, 79–89.

Harrison, T.M., Watson, E.B., 1983. Kinetics of zircon dissolution and zirconium diffusion in granitic melts of variable water content. Contrib. Min. Petrol. 84, 66–72.

Heier, K.S., 1973. Geochemistry of granulite facies rocks and problems of their origin. Phil. Trans. R. Soc. Lond. A273, 429–442.

Herz, N., 1984. Rock suites in Grenvillian terrane of the Roseland district, Virginia; Part 2. Igneous and metamorphic petrology. In: M.J. Bartholomew, E.R. Force, A.K. Sinha, N. Herz (Eds.), The Grenville Event in the Appalachians and Related Topics. Geological Society of America Special Paper, 194: 200–214.

Herz, N., Force, E.R., 1984. Rock suites in Grenvillian terrane of the Roseland district, Virginia; Part 1. Lithologic relations. In: M.J. Bartholomew, E.R. Force, A.K. Sinha, N. Herz (Eds.), The Grenville Event in the Appalachians and Related Topics. Geological Society of America Special Paper, 194: 187–200.

Hudson, T.A., 1981. Geology of the Irish Creek tin district, Virginia Blue Ridge. Unpublished M.S. Thesis, University of Georgia, Athens, GA, 144 pp.

Huang, W.L., Wyllie, P.J., 1973. Melting relations of muscovite-granite to 35 kbar as a model for fusion of metamorphosed subducted oceanic sediments. Contrib. Min. Petrol. 42, 1–14.

Janardhan, A.S., Newton, R.C., Hansen, E.C., 1983. Transformation of Peninsular gneiss to charnockite in southern Karnataka. In: S.M. Naqvi and J.J.W. Rogers (Editors), Precambrian of South India. Geol. Soc. India Mem. 4, 417–435.

Kay, R.W., Mahlburg Kay, S., 1986. Petrology and geochemistry of the lower continental crust: an overview. In: J.B. Dawson, D.A. Carswell, J. Hall, K.H. Wedepohl (Eds.), The Nature of the Lower Continental Crust. Geol. Soc. Spec. Publ., 24: 147–159.

Kilpatrick, J.A., Ellis, D.J., 1992. C-type magmas: igneous charnockites and their extrusive equivalents. Trans. R. Soc. Edinburgh: Earth Sciences 83, 155–164.

Lambert, I.B., Heier, K.S., 1967. The vertical distribution of uranium, thorium, and potassium in the continental crust. Geochim. Cosmochim. Acta 31, 377–390.

Mezger, K., Essene, E.J., van der Pluijm, B.A., Halliday, A.N., 1993. U-Pb geochronology of the Grenville Orogen of Ontario and New York: constraints on ancient crustal tectonics. Contrib. Min. Petrol. 114, 13–26.

Mitra, G., Elliott, D., Deformation of basement in the Blue Ridge and the development of the South Mountain cleavage, In: D.R. Wones (Editor), Proceedings, The Caledonides in the USA, I.G.C.P. Project 27: Caledonide Orogen: Virginia Tech. 1980. Department of Geological Sciences, Memoir 2, 307–311.

Mitra, G., Lukert, M.T., 1982. Geology of the Catoctin-Blue Ridge anticlinorium in northern Virginia, In: P.T. Little (Ed.), Central Appalachian Geology, NE-SE GSA '82 Field Trip Guidebooks. American Geological Institute, pp. 83–108.

Nash, W.P., Crecraft, H.R., 1985. Partition coefficients for trace elements in silicic magmas. Geochim. Cosmochim. Acta 49, 2309–2322.

Patiño Douce, A.E., Johnston, A.D., 1991. Phase equilibria and melt productivity in the pelitic system: implications for the origin of peraluminous granitoids and aluminous granulites. Contrib. Min. Petrol. 107, 202–218.

Patiño-Douce, A.E., Beard, J.S., 1995. Dehydration-melting of biotite gneiss and quartz amphibolite from 3 to 15 kbar. J. Petrol. 36, 707–738.

Pettingill, H.S., Sinha, A.K., Tatsumoto, M., 1984. Age and origin of anorthosites, charnockites, and granulites in the central Virginia Blue Ridge. Nd and Sr isotopic evidence. Contrib. Min. Petrol. 85, 279–291.

Rudnick, R.L., Fountain, D.M., 1995. Nature and composition of the continental crust: A lower crustal perspective. Rev. Geophys. 33 (3), 267–309.

Rudnick, R.L., McLennan, S.M., Taylor, S.R., 1985. Large ion lithophile elements in rocks from high-pressure granulite facies terranes. Geochim. Cosmochim. Acta 49, 1645–1655.

Sighinolfi, G.P., 1971. Investigations into deep crustal levels: fractionating effects and geochemical trencs related to high-grade metamorphism. Geochim. Cosmochim. Acta 35, 1005–1021.

Sinha, A.K., Bartholomew, M.J., 1984. Evolution of the Grenville terrane in the central Virginia Appalachians. In: M.J. Bartholomew, E.R. Force, A.K. Sinha, N. Herz (Editors), The Grenville Event in the Appalachians and

Related Topics. Geological Society of America Special Paper, 194: 175–186.

Stähle, H.J., Raith, M., Hoernes, S., Delfs, A., 1987. Element mobility during incipient granulite formation at Kabbaldura, southern India. J. Petrol. 28, 803–834.

Streckeisen, A., 1974. How should charnockitic rocks be named? In Centenaire de la Société Géolgogique de Belgique. Géologie des Domaines Cristallins, Liège, pp. 349-360.

Streckeisen, A., 1976. To each plutonic rock its proper name. Earth Sci. Rev. 12, 1–33.

Taylor, S.R., McLennan, S.M., 1985. The Continental Crust: Its Composition and Evolution. Blackwell Scientific, Oxford, 312 pp.

Taylor, S.R., McLennan, S.M., 1995. The geochemical evolution of the continental crust. Rev. Geophys. 33 (2), 241–265.

Tollo, R.P., Hutson, F.E., 1996. 700 Ma rift event in the Blue Ridge province of Virginia: A unique time constraint on pre-Iapetan rifting of Laurentia. Geology 24, 59–62.

Watt, G.R., Harley, S.L., 1993. Accessory phase controls on the geochemistry of crustal melts and restites produced during water-undersaturated partial melting. Contrib. Min. Petrol. 114, 550–566.

Weaver, B.L., Tarney, J., 1983. Elemental depletion in Archaean granulite facies rocks. In: M P. Atherton, C.D. Gribble (Eds.), Migmatites, Melting and Metamorphism. Shiva Pub. Ltd, Cheshire, pp. 250–263.

White, A.J.R., Chappell, B.W., 1977. Ultrametamorphism and granitoid genesis. Tectonophysics 43, 7–22.

Wickham, S.M., 1992. Fluids in the deep crust – petrological and isotopic evidence. In: D.M. Fountain, R. Arculus, R.W. Kay (Eds.), Continental Lower Crust. Developments in Geotectonics 23. Elsevier, Oxford, pp. 391–421.